Università
Ca'Foscari
Venezia

CORSO DI DOTTORATO DI RICERCA IN

SCIENZA E GESTIONE DEI CAMBIAMENTI CLIMATICI

Ciclo XXXI

Tesi di Ricerca

Global climate impacts of the Atlantic Multidecadal Variability: a model-based approach

Coordinatore del Dottorato:

Prof. Carlo Carraro

Supervisori:

Dr. Alessio Bellucci

Dr. Dorotea Iovino

Dottorando:

Dario Nicoli'

Matricola 956215

Il divertimento della ricerca scientifica
è anche trovare sempre altre frontiere da superare,
costruire mezzi più potenti d'indagine,
teorie più complesse,
cercare sempre di progredire
pur sapendo che probabilmente
ci si avvicinerà sempre di più a comprendere la realtà,
senza arrivare mai a capirla completamente.

Margherita Hack
[1922 - 2013]

Abstract

The Atlantic Multidecadal Variability (AMV) is associated to a natural, low-frequency (roughly 40 - 80 years) fluctuation of the observed North Atlantic sea surface temperature (SST). Several components of the climate system are modulated by the AMV, even far from the North Atlantic Ocean, such as tropical-wide rainfall, Atlantic storm track, Indian summer monsoon and, basically, large-scale circulation in the Northern Hemisphere. Nevertheless, our understanding of the impacts and mechanisms at stake is limited by the AMV relatively short observational record and, in this context, climate models play a crucial role.

This thesis assesses the climate impact of the positive and negative phase of the AMV in a suite of idealized experiments in which, following the Decadal Climate Prediction Project protocol, the North Atlantic SST is restored towards an estimation of the observed AMV anomalies. We use the CMCC-CM2-SR5 coupled model. To validate model results, a comparison with previous literature, and in particular with a set of new simulations performed by the CNRM-CM5 coupled-model, is presented in the global climate assessment.

Boreal summer response shows enhanced rainfall over the equatorial belt, including the semiarid Sahel region, Central America and Maritime Continent, consistently with a northward shift of the Inter-Tropical Convergence Zone which, in turn, modifies the Walker circulation. During boreal winter, the AMV

projects the Pacific Ocean into the negative phase of the Interdecadal Pacific Oscillation. Significant warming is also found over the semiarid Sahel region, Middle East and Indian sub-continent. Interestingly, despite the seasonal responses, some features persist throughout the year such as deep convection over the Western Tropical Pacific, characterized by warm and wet anomalies.

The behavior of the eddy-driven jet stream under AMV-induced variability is also analyzed. The imposed pattern of SST decreases the meridional temperature gradient in the North Atlantic since the AMV-related largest anomalies straddle an area characterized by a strong baroclinicity. A positive AMV phase indeed shifts southward the eddy-driven jet stream, mirroring in an increase of the European precipitation, associated to an anomalous transport of moist air along the modified jet path.

Furthermore, we address the relationship between the AMV and the Tropical Pacific due to the Atlantic inter-hemispheric imbalance. From warm North Atlantic Ocean, an ascending flow reaches the upper troposphere and mostly sinks in the equatorial Central Pacific, linking the two basins. Over the subsidence zone, low-level winds zonally diverge inducing an atmospheric double-cell circulation, with upward flows over the Indonesia and Mexico, and an oceanic La Niña-like response along the Tropical Pacific. These findings support the idea that the "hiatus" in the global mean temperature rise, occurred in the early 2000s, is a lagged Pacific response to a cold-to-warm AMV phase transition.

Contents

Motivation and Thesis Outline

The North Atlantic Ocean plays an essential role in the global climate system, accounting for ~25% of the global ocean-atmosphere meridional heat transport. Local sea surface temperatures (SST) modulate the Earth climate on a wide range of time scales, from interannual to decadal, up to millennial. Low-frequency SST fluctuations occurring over 40-80 years are termed as the Atlantic Multidecadal Oscillation (AMO) [Kerr 2000]. However, given the lack of a regular periodicity in the historical AMO record, the climate community often refers to the AMO as the Atlantic Multidecadal Variability (AMV). The literature provides several methods to identify the AMV. A first, elementary definition regards the variations of the North Atlantic SST on multidecadal timescale that are not consistent with the long term warming trend [Enfield et al. 2001]. Another definition is based on the idea that the AMV consists in the departure of the averaged North Atlantic SST from to global SST mean [Trenberth and Shea 2006]. This thesis follows the most recent definition which considers the AMV as the internally-driven component of the multidecadal North Atlantic SST variability, after removing the contribution of the external forcings [Ting et al. 2009]. The drivers are still a matter of debate for climatologists which are basically divided in two schools of thought: those who argue that the AMV is essentially driven by processes that are internal to the ocean system (notably, multi-decadal changes in the meridional overturning circulation) [e.g. Zhang et al. 2016, Delworth et al. 2017] in opposition to those who claim that external forcings play an equally important role [e.g. Booth et al. 2012, Bellucci et al. 2017].

In the context of the AMV process understanding, climate models are key since the observed historical record is too short (~120 years) in relation to its dominant variability timescale, to allow a robust statistical evaluation based exclusively on the instrumental data (Figure 1.1). Paleoclimate reconstructions may contribute to fill the lack of direct observations, even if their distribution in time and space is very scattered [e.g. Gray et al. 2004]. Models also allow tackling the challenging task of identifying and quantifying the footprint of the AMV on the climate system both within and outside the Atlantic sector.

Interestingly, the AMV is associated with a world-wide range of hydro-climatic impacts, affecting regional scale changes in air temperature, precipitation and atmospheric circulation. These include above-normal warming over North America [e.g. Sutton and Hodson 2005] and the Euro-Mediterranean sector [e.g. Sutton and Dong 2012, Mariotti and Dell'Aquila 2012, equatorial precipitation anomalies [e.g. Knight et al. 2006], Atlantic hurricane activity [e.g. Trenberth and Shea 2006], Sahelian and Indian Monsoon [e.g. Zhang and Delworth 2006, Wang et al. 2012], mid-latitude atmospheric circulation [e.g. Davini et al. 2015, Woollings et al. 2018] and deep convection over the West Tropical Pacific [Sun et al. 2017]. The aforementioned teleconnections stress the need for further investigating the role of AMV in modulating global climate variability.

The motivation behind this thesis is to improve the knowledge of the AMV impacts and to provide a model-based assessment through a pioneering experimental approach. Among other aspects, this work focuses on the uncertainty related to the European climate during wintertime through an analysis of the eddy-driven jet position under an anomalous equator-to-pole SST gradient, typical of the AMV polarities [e.g. Woollings 2010]. Another important focus of this thesis is the teleconnection between

the North Atlantic and the Tropical Pacific, which is investigated in light of the most recent findings [e.g. Kucharski et al. 2016a].

Methodologically speaking, this study follows the experimental protocol outlined in the Decadal Climate Predictions Project (DCPP – Component C1) [Boer et al. 2016], using the state-of-the-art CMCC-CM2-SR5 global climate model [Cherchi et al. 2018]. The innovative approach lies in using idealized experiments to explore the impacts and the mechanisms at stake: an estimate of the AMV-related SST anomalies is imposed over the North Atlantic basin, while the remaining domain can freely evolve. This approach allows to isolate the global climate response to the internal low-frequency SST variability in the North Atlantic.

The thesis is organized as follows: chapter 1 introduces the AMV and its impact on global scale as documented in literature, chapter 2 focuses on the methodology, chapter 3 assesses the global, seasonal response to the AMV, chapter 4 and 5 analyze two physical mechanism induced by the AMV, such as the meridional shift of the eddy-driven jet during wintertime and the Tropical Pacific response associated with the Atlantic-Pacific trans-basin atmospheric bridge, respectively. Final conclusions are provided in chapter 6.

1 – The Atlantic Multidecadal Variability

1.1 Multidecadal variability of the North Atlantic sea surface temperature

On multidecadal timescales, the observed large-scale variability in the North Atlantic SST, has been referred to the Atlantic Multidecadal Oscillation, AMO (or AMV) [Kerr, 2000, Trenberth and Shea 2006, Knight et al. 2006, Ting et al. 2009, Ting et al. 2011]. The AMV is associated to a natural fluctuation of the basin-wide SST between a warm and a cold state, with a preferential period of roughly 40 – 80 years as detected in instrumental data [Enfield et al. 2001, Sutton and Hodson 2005, Ting et al. 2011, Meehl et al. 2011] as well as in paleo-proxy records [Gray et al. 2004, Chylek et al. 2012, Wang et al. 2018, Steiger et al. 2018]. In this study, the AMV index is basically obtained subtracting the estimated forced component from the detrended North Atlantic SST observations [Ting et al. 2009, Ting et al 2011], as described in the DCPP protocol (for further details see Chapter 2). The corresponding pattern (Figure 1.2) reveals a range of variability of about 0.4°C, characterized by positive anomalies over the whole North Atlantic, with maxima over the subpolar gyre, the Gulf Stream area, and along the Eastern Tropical Atlantic branch from western Africa to North-East Brazil [Knight et al. 2006, Trenberth and Shea 2006, Ting et al. 2009]. Furthermore, the SST anomalies endure throughout the year. The observed record (1870-2013) presents two anomalously cold periods (1900-1920 and 1970-1990) and three anomalously warm periods, one at the beginning of the record, at the half of the 20th century (1930-1960), and an ongoing one that started in the 90's (Figure 1.1). The origin and the mechanism by which the AMV arise are still unclear and under debate. Up to the last decade, the main paradigm has involved the role of the internal multidecadal

variability of the Atlantic Meridional Overturning Circulation (AMOC) in driving the multidecadal SST anomalies over the northern part of the Atlantic region with a lead time of a few years [e.g. Knight et al. 2006, Barcikowska et al. 2017]. In fact, many modeling studies are able to reproduce AMV-like pattern showing that the AMOC can modulate the decadal variations of SST, coherently with changes in heat content and salinity [Gastineau and Frankignoul 2012, Wang et al. 2014, Ba et al. 2014], even if amplitudes and frequencies differ significantly among the models [Otterå et al. 2010, Menary et al. 2015]. Zhang and Wang [2013] found that a stronger (weaker) AMOC induces a positive (negative) AMV phase through an anomalously higher (lower) northward (southward) heat transport which, as a negative feedback, leads to a slowdown (a speed up) of the AMOC by changing in the meridional density gradient.

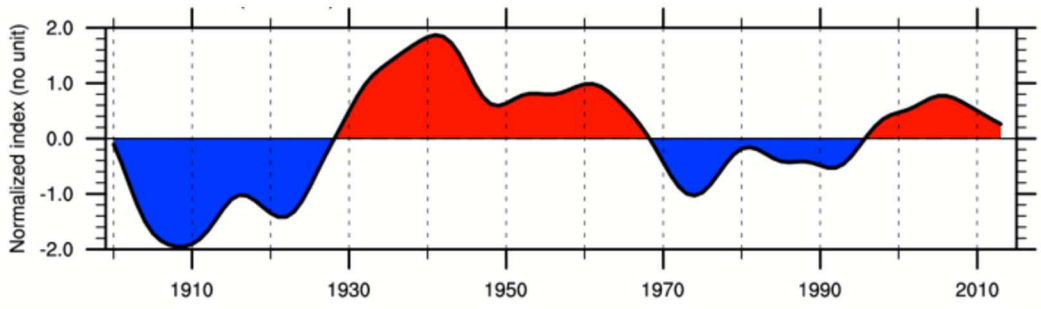

Figure 1.1. *Historical internal component of the of the observed Atlantic Multidecadal Variability Sea Surface Temperature following the definition by Ting et al. [2009]. Data before the year 1900 are used for the estimation of the AMV index. Figure from Boer et al. 2016*

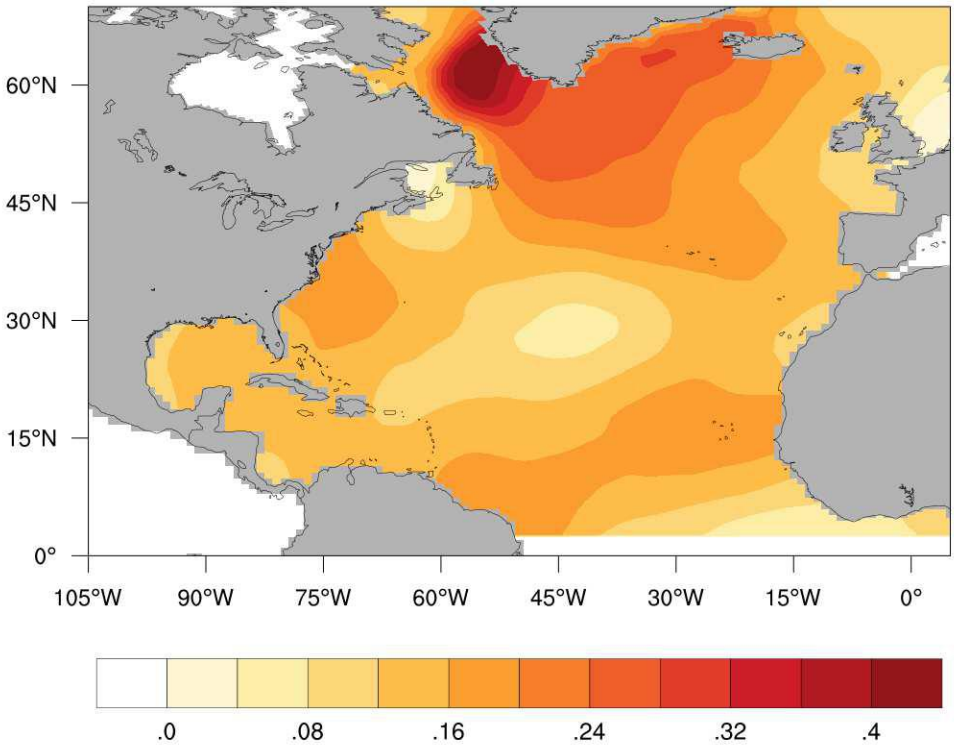

***Figure 1.2**: Spatial pattern of the observed Atlantic Multidecadal Variability Sea Surface Temperature anomalies ($°C/\sigma_{AMV}$) computed from annual regression of the Extended Reconstructed Sea Surface Temperature version 4 (ERSSTv4) after removing the forced component [Huang et al. 2015]. Data provided by Decadal Climate Prediction Project - component C [Boer et al. 2016].*

Even though most studies suggest that the AMV is mainly driven by internal variability of the Atlantic atmospheric and ocean system [Ting et al. 2009, Ting et al. 2011, Zhang et al. 2016, Delworth et al. 2017], external contributions cannot be neglected. Booth et al. [2012] attributed a potential role for anthropogenic aerosols using a single model. Zhang et al. [2013] replied that the Booth's model is biased by an excessive response to aerosol effects. Moreover, Clement et al. [2015] found that the pattern of AMV can be produced in a slab ocean model that does not include ocean

circulation variation, but only changes in air temperatures and winds (i.e. slab ocean model). Several studies replied to this article [Zhang et al. 2016, Delworth et al. 2017] sustaining that surface heat fluxes are not well investigated. Bellucci et al. [2017] claimed that the North Atlantic SST response to aerosol forcings diverges among the CMIP5 models. Clustering the models as a function of their response, they showed that some models present skill on the North Atlantic SST in historical and anthropogenic-only ensemble simulations, proposing that a portion of the observed AMV was driven by anthropogenic aerosol forcing. Nevertheless, the onset of the AMV is still a matter of debate.

1.2 Global Impacts of the Atlantic Multidecadal Variability

The wide-ranging impacts of the AMV has been extensively analyzed by the climate science community [e.g. Knudsen 2000, Knight et al. 2006, Zhang and Delworth 2006, Edwards et al. 2013, Gastineau and Frankignoul 2015, Steinman et al. 2015, Ruprich-Robert et al. 2017].

Last-century observed variability of the North Atlantic SST has primarily affected the entire ocean basin and the surrounding areas such as the North Atlantic and European (NAE) region with higher anomalies during Boreal summer [Sutton and Hodson 2005, Knight et al. 2006, Arguez et al. 2009]. Model studies also suggest enhanced Surface Air Temperature (SAT) over the subpolar Gyre (SPG), with a characteristic horse-shoe shape, and over the Eastern Tropical Atlantic which resembles the spatial pattern of the AMV [Kerr 2000, Ting et al. 2011, Ruprich-Robert et al. 2017]. At multidecadal timescales, the European climate variability is mainly driven by the AMV [Sutton and Hodson 2012] and shows weak seasonal changes especially in

terms of air temperature [Davini et al. 2015, Terray and Cassou 2002, Häkkinen et al. 2011]. Sutton and Dong [2012] found similar June-to-August SAT patterns between the last two historical warm phases (1930 – 1960 and 1996 – 2010) with positive anomalies over Western-Southern Europe [e.g. Hurrell and Folland 2002], Northern Africa [e.g. Folland et al. 1986, Knight et al. 2006] and the Mediterranean basin [e.g. Marullo et al. 2011, Mariotti and Dell'Aquila 2012]. Heat-wave events are positively correlated to the AMV over Western Europe [Cassou et al. 2005]. Precipitation field reveals a clear climate dipole, characterized by enhanced rainfall over Northern Europe and reduced rainfall over Southern Europe [Cassou et al. 2004, Sutton and Hodson 2005]. A collateral effect involves forest productivity in South-western Europe where trees photosynthetic activity is directly proportional to multidecadal SAT anomalies [Madrigal-Gonzalez et al. 2017].

During a positive phase of the AMV, cyclonic pressure anomalies, coherent to surface wind anomalies over the Atlantic and Europe [Knight et al. 2006, Sutton and Hodson 2005, Sutton and Dong 2012], resemble a Gill-like response to anti-symmetric heating [Gill 1980]. An anomalous extratropical heating alters the inter-hemispheric energy balance with southward energy transport across the equator and northward shift of the Hadley cell and the Inter-Tropical Convergence Zone (ITCZ) [e.g. Donohoe et al. 2014]. This link is evident in the National Centers for Environmental Prediction – National Center for Atmospheric Research (NCEP–NCAR) reanalysis where 41% of the equatorial Hadley Cell variability and 74% of the Atlantic tropospheric temperature asymmetry are explained by the AMV index [Green et al. 2017]. In Lyu and Yu [2017], neglecting the global mean SST contribution, observed and preindustrial CMIP5 precipitation patterns share the aforementioned shift, with an enhanced rainfall over the northern part of the tropical belt. During Boreal summer, increased rainfall has been recorded over the Sahel [Knight et al. 2005, Knight et al. 2006, Ting et al. 2011]. The

warm AMV phase triggers a positive feedback: ITCZ shift enhances climatological rainfall, via increased Atlantic moisture transport by southwesterly wind anomaly. Over the Sahel, precipitation increases at the expense of the mineral aerosols. Damping this Atlantic source of dust, more solar radiation can reach the oceanic surface and heats the tropical SST, closing the loop [Wang et al. 2012]. This mechanism is also reinforced by the decrease of low cloud fraction due to mid-latitude ocean warming [Yuan et al. 2016]. Since Tropical SST is one of the main features used to characterize a favorable environment for the hurricanes development therefore, it is expectable Atlantic-hurricane events have a strong positive correlation to the warm phase of the AMV [e.g. Goldenberg et al. 2001, Trenberth and Shea 2006, Knight at al. 2006, Zhang and Delworth 2009]. Weaker vertical wind shear, through reduction of the meridional temperature gradient, also contributes to a higher number of hurricane events and can be reinforced by multidecadal dust drop over the tropical Atlantic [Wang et al. 2012].

The regional behavior of the seasonal NAE response to AMV signal may be explained by changes in large-scale atmospheric flows [Davini et al. 2015, O'Reilly et al. 2017]. According to Woolings et al. [2018], based on the ERA-Interim reanalysis [Dee et al. 2011] and on several coupled/uncoupled climate model simulations with different horizontal resolutions, the North Atlantic Jet (NAJ) can meridionally shift because of a weakening of the jet speed, considering a reduction of the basin-wide meridional SST gradient, as in the case of the positive AMV. This displacement from the mean-state position has serious climate impact on the Euro-Atlantic sector, like more frequent negative North Atlantic Oscillation (NAO) patterns and atmospheric blocking events [e.g. Häkkinen et al. 2011, Peings and Magnusdottir 2016]. The former is a well-known mode of variability of the Northern Hemisphere estimated by the Sea-Level-Pressure (SLP) difference between the Iceland Low and the Azores High [e.g. Hurrell et al. 2003]. When the SLP gradient decreases, a negative NAO is occurring tied to fewer and weaker

storms crossing the winter Atlantic, bringing moist air into the Mediterranean. The existence of the AMV/NAO interplay has been demonstrated in several studies, where the most part of the NAO-like signature is driven to a large extent by the tropical part of the AMV [Terray and Cassou 2002, Gastineau and Frankignoul 2015, Peings and Magnusdottir 2014, Peings and Magnusdottir 2016]. Davini et al. [2015] have argued that two different dynamics act during a positive phase of the AMV:

1. The barotropic mechanism: a Gill-like pattern leads to a decrease of the shear of the zonal wind (barotropic shear), affecting the position of the jet maximum and the Rossby-wave breaking occurrence. This, in turn, fosters a negative NAO-like response and the subsequent tropic-ward shift of the North Atlantic eddy-driven jet stream.
2. The baroclinic mechanism: the reduced basin-wide SST gradient due to extra-tropical warming decreases the low-level baroclinicity by means of a decline of the maximum Eady growth rate, attenuating jet speed and pushing the jet stream towards lower latitudes.

Continental America represents a key-region for the global hydroclimatic system. During warm AMV phases, positive SAT anomalies affect the North-American summer [McCabe et al. 2004, Sutton and Hodson 2005, Ting et al. 2011, Ruprich-Robert et al. 2018], associated with a reduction of Great Lakes ice cover [Wang et al. 2018]. Decadal dry periods characterize the Eastern U.S., with observed decrease of precipitation over California in contrast to the wet tropical regions such as the Caribbean, Southwestern U.S. and the Gulf of Mexico associated with the ITCZ meridional-shift influence [Sutton and Hodson 2005]. Consistent with previous results, Enfield [2001] argued that a decreased rainfall deeply modified the river flows in North America by 10% to 40% of the climatological variability, as in the case of Midwest droughts in the first half of the 20th century. Dry periods characterize also the North

East Brazilian region on March-to-May period [Knight et al. 2006, Ting et al. 2011] with altered regimes of the Amazon river, reduced soil moisture and enhanced tree-mortality rates [Davidson et al. 2012].

The Indo-Pacific response to the observed warm AMV leads to negative temperature anomalies over the equatorial band, projecting SST towards a negative IPO-like (Interdecadal Pacific Oscillation) phase [Sutton and Hodson 2006, Ting et al. 2011, Barcikowska et al. 2017]. Interestingly, Kucharski et al. [2011] showed that the 20th-century Atlantic warming may have reduced and eventually fostered the generation of a Pacific La-Niña-like feature via an atmospheric bridge, cooling the eastern side of the Pacific. McGregor et al. [2014] revealed a Walker circulation intensification and a trade winds reinforcement which have contributed to the current precipitation anomalies (e.g. East U.S. drought). Li et al. [2016] emphasized the Atlantic role in initiating the tropical-wide teleconnection. They analyzed, using an atmospheric model coupled with a slab ocean model, the mechanisms behind the tropical-wide SST dipole pattern, with cooling over the tropical Eastern Pacific and warming over the Indo-Western Pacific, supported by the observed field [Barcikowska et al. 2017] and other climate models [Kucharski et al. 2016a, Kucharski et al. 2016b, Zanchettin et al. 2016]. The resulting zonal SST gradient may also generate a la-Nina-like response, altering the thermocline, and a further deep convection over the western boundary of the due to wind convergence, which powers the Bjerknes positive feedback [Bjerknes 1969]. Sun and co-workers [2017] described the decadal AMV-WTP (Western Tropical Pacific) teleconnection as follows: a positive AMV, analogous to Gill anti-symmetric heating off the equator, entails cyclonic surface wind anomalies and upward flux over the North Atlantic, which is balanced by a downward flux in the North Pacific. The anti-cyclonic response weakens the Aleutian low causing easterly wind anomalies over the Subtropical North Pacific (SNP), i.e. weakening the mean westerlies. Wind changes

causes a damping of the Wind-Evaporation-SST (WES) feedback [Xie and Philander 1994] over the SNP, which, in turn, warms the local SST (Figure 1.3a). This warming induces an anomalous cyclonic circulation along with a decrease of the mean SLP over the WTP. The WTP teleconnection further increases the local SST by the development of a SST-SLP-cloud-longwave radiation feedback (Figure 1.3b). They basically argued that the anomalous SST warming involves a negative SLP anomaly, enhancing the cloud cover. This prevents the longwave heat loss from the ocean surface and increase the WTP SST, closing the positive feedback.

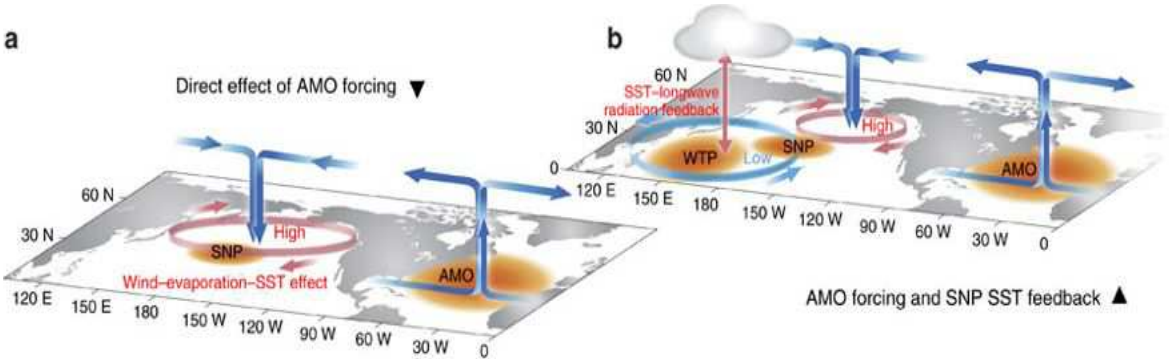

Figure 1.3. AMV-WTP teleconnection. (a)The AMV (or AMO) warming produces atmospheric deep convection and subsequent subsidence in the North Pacific Ocean, associated to an anomalous anti-cyclonic circulation which increases the SST over SNP, via WES feedback. (b) The resulting SNP warming alters the local wind circulation by an anomalous low pressure center over the WTP. The teleconnection further feeds this warming through SST-SLP-cloud-longwave radiation feedback.

The AMV-related atmospheric circulation anomaly also influences the ISM, with above-normal rainfall during warm AMV phase [Goswami et al. 2006, Krishnamurthy and Krishnamurthy 2016, Ruprich-Robert et al. 2017]. This observed teleconnection can

be explained by two different mechanisms: the aforementioned Atlantic-Pacific linkage and the Rossby wave train generated by the Atlantic warming over Eurasia. Equatorial African wind anomalies reinforce the south-westerlies over the Indian region associated to an increase of meridional tropospheric temperature gradient and consequential bolstering of the ISM rainfall [Goswami et al. 2006, Joshi and Rai 2015]. A recent CMIP5 historical-run analysis has revealed that the multidecadal Indian observed precipitation pattern can be reproduced by just 16 models out of 30. All the models, that fail in reproducing the AMV-ISM teleconnection, are not able to catch the AMV-associated change of the Walker circulation [Joshi and Ha 2018].

The Arctic ocean is strongly connected to the Atlantic basin with almost 9 Sv of warm, salty Atlantic water inflowing through the Fram Strait and the Barents Sea Opening, with a significant role of the AMV in modulating also the decadal Arctic sea-ice trend [Beszczynska-Möller et al. 2011]. Paleo-climate records (marine sediments, tree rings and ice cores) clearly reveal in-phase correlation between sea-ice variability and multidecadal North Atlantic SST fluctuations, mainly in the Greenland Sea and Kara Sea and accelerated melting rate during a cold-to-warm transition [Eldevik et al. 2009, Frankcombe et al. 2010, Kinnard et al. 2011, Drinkwater et al. 2013, Miles et al. 2014]. The AMV signal in the Arctic is also evident in modeling studies, explaining one-third of the September sea-ice extent decline in the satellite era [Day et al. 2012]. Polar amplification (the ratio of the Arctic and global temperature rate of change) has also an AMV-like oscillation, although it was 4-times higher in the past warm phases than to the most recent one (current polar amplification factor is between 2 and 3) [Chylek et al. 2009]. On the Siberia region, which is one of main land source of fresh water for the Arctic ocean, the AMV covaries with the detrended Siberian warm season precipitation index due to extra-moisture transport by wind anomalies [Sun et al. 2015].

Anyhow, the large literature highlights the role of the AMV in modulating the climate system, along with marked changes in air temperature, precipitation and atmospheric circulation, even far from the Atlantic Ocean. Furthermore, the uncertainty related to the impact assessment suggests the need of a multi-model framework to overcome the model dependency of the results. In this context, the DCPP may be a useful tool to address different research groups towards a common effort. This thesis represents the first step in that direction, investigating on the AMV-associated impacts and mechanisms by a new, groundbreaking methodology.

2 – Methodology

2.1 Decadal Climate Prediction Project

The DCPP is a coordinated multi-model effort which involves more than 15 international institutes within the World Climate Research Programme (WCRP), and aims to investigate climate prediction, predictability and variability on annual, multi-annual to decadal timescales [Boer et al. 2016]. The DCPP contributes to the sixth Coupled Model Intercomparison Project (CMIP6), to WCRP Grand Challenge on Near Term Climate Prediction and, potentially, to the Sixth Assessment Report of the Intergovernmental Panel on Climate Change.

Moreover, the DCPP is intended to make skillful forecasts and predictions on these timescales using the latest generation of climate models and statistical approaches. Involving many scientific and practical issues, the project is organized in four components as follows:

A. *Hindcasts*: the Component A includes an archive of retrospective forecasts (hindcast) for improving decadal prediction and annual-to-decadal forecast through the assessment of the predictive skills on these time scales.

B. *Forecasts*: the Component B lays the foundation for potential operational forecast system using the ongoing production of experimental quasi-operational decadal climate predictions.

C. *Predictability, mechanisms and Case Studies*: the Component C is aimed at understanding of the decadal, physical mechanisms by predictive skills and to identification of the model gaps in initialization and ensemble generation. Furthermore, a number of case studies are considered to shed the light on

particular climatic events (e.g. climate shift, hiatus, etc.) along with broader issues which arise.

Specifically, the section C1, "*accelerated and retarded rates of global temperature change and associated regional climate variations*", considers the role of the multidecadal North Atlantic and North Pacific SSTs in driving regional changes by means of idealized experiments. This thesis assesses the idealized climate impacts of the positive and negative AMV phases following the sections C1.2 and C1.3, respectively, and focusing on the regional imprints.

2.2 Estimation of the internal component of the AMV

The AMV index and its spatial pattern are provided by the DCPP protocol, based on the ERSSTv4 presented in Huang et al. [2015]. ERSTTv4 is a monthly SST collection on global scale which includes in situ data from the International Comprehensive Ocean-Atmosphere Dataset release 2.5 from 1854 to present, with a horizontal resolution of 2° x 2°. The internal component of the observed decadal variability has been computed as the residual of the annual mean of the global, observed SST and the external component that includes natural (solar radiation and volcanos activity) and anthropogenic (aerosol and GHG) signals. The time evolution related to the external contribution is obtained starting from the first Principal Component ($PC1_{for}$) of the signal-to-noise maximizing Empirical Orthogonal Function (EOF) analysis applied to SST from the CMIP5 historical runs (for the 1870-2005 period) and Representation Concentration Pathway 8.5 (RCP8.5) simulations (for the 2006-2013 period) [Ting et al. 2009]. The regression of the observed SST onto $PC1_{for}$ is used to

estimate the spatial pattern of the forced component of the ERSSTv4, hereafter SST_{for} (Figure 2.1).

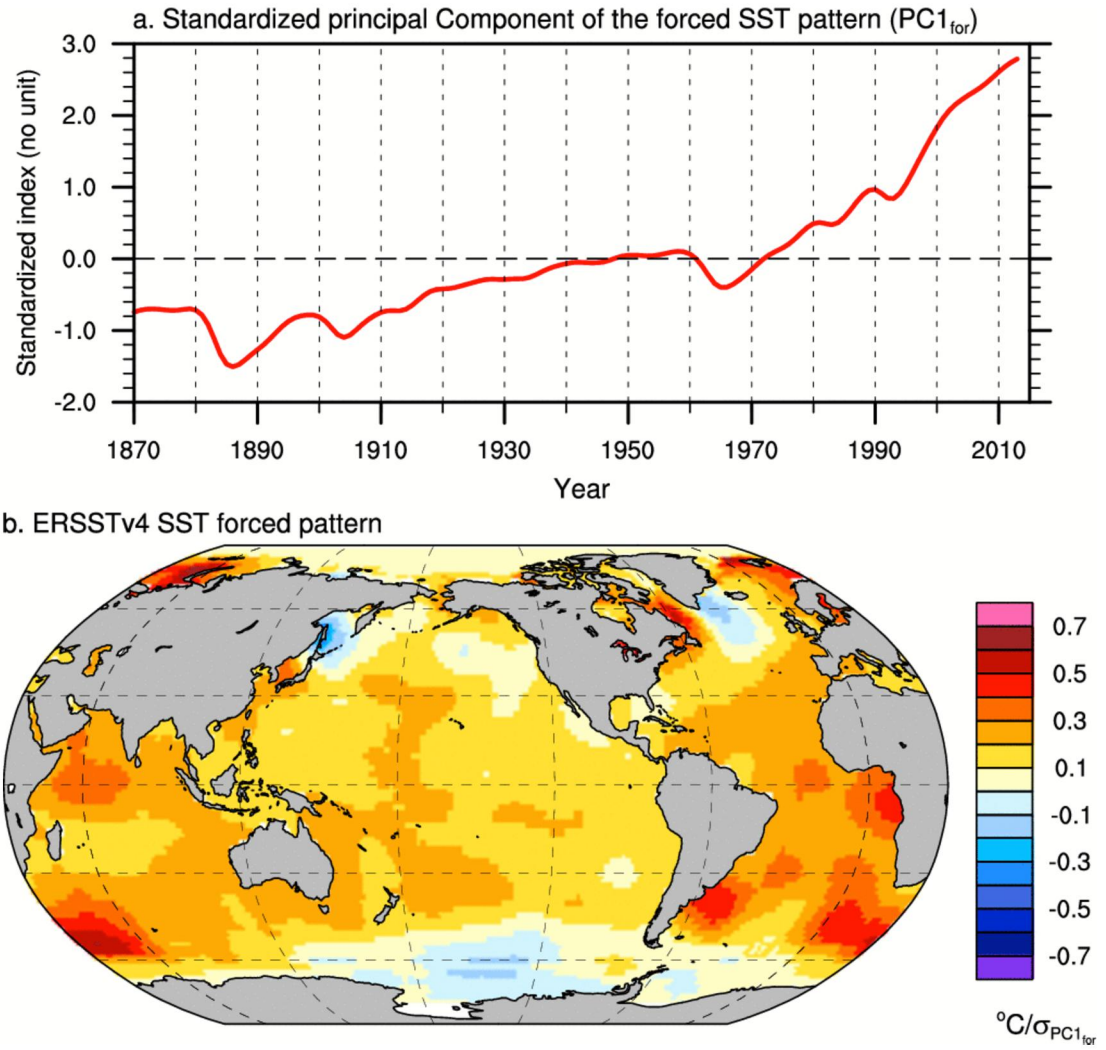

Figure 2.1: a) Standardized first Principal Component of the forced contribution estimated from ERSSTv4 dataset for 1870-2013 period [method by Ting et al. 2009] b) ERSST4 SST pattern computed from the regression of the observed SST onto $PC1_{for}$. Contour interval is 0.1°C/σ_{PC1for}. Figure from Tech. Note I, Boer et al. 2016.

The internal component of the historical, global SST (SST_{int}) is estimated by subtracting the forced component ($PC1_{for}$ x SST_{for}) from the observed SST. The SST_{int}

is spatially averaged over a North Atlantic sector (75°W – 7.5°E and 0° – 60°N, neglecting the Mediterranean and Baltic seas). A second-order zero-phase Butterworth filter is applied with a cutoff period of 10 years, obtaining the historical AMV index. The AMV spatial pattern results from regressing the global SST_{int} on the AMV index for the sub-period 1900–2013 when the observations are more reliable [Tech. Note I, Boer et al 2016].

2.3 Experimental setup

To assess the AMV climate impact on global scale, the CMCC–CM2-SR5 model is used [Cherchi et al. 2018, Fogli and Iovino 2014], which is a new climate system model developed at the Euro-Mediterranean Centre on Climate Change (CMCC) Foundation. Its core is based on the Community Earth System Model (CESM) except for the ocean component, which is represented by the Nucleus for European Modelling of the Ocean (NEMO). The physical component of the atmospheric model is the Community Atmospheric Model version 5 (CAM5) [Naele et al. 2012]. CAM5 is used in Finite-Volume dynamical-core mode in which the discretization is local and in physical space. The horizontal discretization is based on a conservative "flux-form semi-Lagrangian" scheme [Lin and Rood 1996, Lin and Rood 1997], while the vertical discretization is defined as "quasi-Lagrangian", i.e. a Lagrangian scheme with a conservative re-mapping. All prognostic variables are updated by the dynamics and subsequently by the physics. CAM5 is characterized by a regular, horizontal grid of 0.9° x 1.25°. The vertical resolution encompasses 30 vertical hybrid levels, 17 of which below 200 hPa to include the lower-stratosphere. The ocean component is NEMOv3.6 [Madec et al. 2016] which is a three dimensional, free-surface, hydrostatic, primitive-equation global ocean general

circulation model. In this study, the grid configuration employs ORCA tripolar grid – a global curvilinear ocean grid which has two poles in the northern hemisphere located over land [Madec and Imbard 1996]. The horizontal mesh has a 1° (~100 km) horizontal resolution with a meridional refinement up to 1/3° in the tropical region. The vertical grid has 50 geopotential levels, ranging from 1 m at the surface to 5900 m at the ocean bottom. The Community Ice CodE is the sea-ice model [Hunke and Lipscomb, 2008], sharing the horizontal grid with the ocean in CMCC-CM2-SR5. The land component is the Community Land Model version 4.5 (CLM4.5) [Oleson et al. 2013], which is able to simulate the physical, chemical and biological processes involving land surface. For this study, the model is used in its "Satellite Phenology" mode, namely the prognostic carbon–nitrogen model is deactivated, and employs the horizontal grid of the atmospheric component. CLM is coupled with the River Transport Model, which routes liquid and ice runoff from the land surface model to the active ocean to simulate a closed hydrologic cycle [Branstetter and Famiglietti 1999].

To isolate the internal variability effects and neglect the anthropogenic and external contributions, all external forcings (such as Greenhouse Gases, solar radiation and tropospheric aerosols) are set at the CMIP6 pre-industrial values, constant at 1850's levels: CO_2 concentration is 284.32 ppm, CH_4 concentration is 808.25 ppb and N_2O concentration is 273.02 ppb.

In order to simulate the AMV impact, the model SST of the North Atlantic Ocean are nudged towards the spatial pattern obtained in the previous section. There are several methods to force the model SST towards given values over a specific area. In the ocean component of the CMCC coupled model, NEMO uses flux formulation to globally restore SST, considering a negative feedback term to be added to the surface non-solar heat flux Q_{ns}^{0}:

$$Q_{ns} = Q_{ns}^{0} + \frac{dQ}{dT}(SST_{MODEL} - SST_{TARGET})$$

where:

- Q_{ns} is the resulting surface non-solar heat flux.
- $\frac{dQ}{dT}(SST_{MODEL} - SST_{TARGET})$ is defined as the heat flux restoring term (hereafter *hfcorr*) which provides a measure of the restoring efficiency.
- $\frac{dQ}{dT}$ is a negative feedback coefficient (γ_T) which indicates the restoring strength. According to the DCPP protocol, this term is fixed at -40 W m^{-2} K^{-1} equal to a relaxation time scale (τ_R) of 60 days for a 50m Mixed-Layer Depth (MLD).
- SST_{MODEL} is the model SST.
- SST_{TARGET} is the target SST which is, in this study, the positive (or negative) 1 standard deviation of the AMV anomalies superimposed to the model climatology.

The selected value for the negative feedback coefficient (γ_T = -40 W m^{-2} K^{-1}) is strongly recommended by the protocol. Given that the higher the coefficient γ_T, the shorter the relaxation timescale for a fixed MLD, a stronger relaxation can carry out to uncontrolled side effects as spurious ocean circulation features and inconsistent heat exchange [Tech. note II, Boer et al. 2016]. The authors also stressed that the restoring efficiency depends on the MLD and, in light of the seasonal and regional behavior of the North Atlantic Ocean, the strength of the surface heat flux correction can vary according to the month and the latitude of the nudging area. To quantify this variability, the temperature Restoring Rate (RR_T) is introduced as the ratio between the feedback coefficient (γ_T) and the constant pressure specific heat (C_P):

$$RR_T = \frac{\gamma_T}{C_P} = \frac{-40\ [^{W}/_{m^2\ K}]}{4184\ \left[^{J}/_{Kg\ K}\right]} \cong -10^{-2}[^{mm}/_{s}] = -864\ \left[^{mm}/_{d}\right] = \frac{MLD}{\tau_R}$$

where γ_T is equal to the protocol value, sea-water C_P is equal to 4184 [J Kg^{-1} K] and RR_T discloses a reference for the restoring evaluation. RR_T also rates the relationship between MLD and τ_R. Strong restoring implies a 10-m mixed layer accounting for a τ_R equal to ~11.5 days while, where there is deep convection (MLD = 1000 m), the restoring is very weak (with $\tau_R \sim 3.2$ years). To check the correct implementation of the regional restoring in the CMCC-CM2-SR5 ocean component, several sensitivity tests have been performed in different areas (North Atlantic Ocean, North Pacific Ocean, Arctic Ocean, Barents Sea and Mediterranean Sea), running both in a standalone (ocean and sea-ice sub systems) and in a fully coupled configuration (including all the model components). Another set of sensitivity experiments has been used to verify the potential occurrence of temperature drift lined to SST restoring over some critical zones, as the SPG. Temperature restoring introduces density anomalies over the SPG: for instance, during a simulated positive phase, warm anomalies tends to stabilize the ocean column reducing the deep ocean convection and generating a weakening of the SPG density. These negative density anomalies may induce a decline in the AMOC and SPG strength, also affecting the poleward ocean heat transport. In the opposite case, imposing cold anomalies over the SPG can lead to a surplus of poleward ocean heat transport [Boer et al. 2016, Ruprich-Robert et al. 2017]. This drift is strongly model dependent [Tech. Note II, Boer et al 2016] and, to verify its occurrence, a mini-ensemble of three members (i.e. simulations with three different initial conditions taken from a multi-century pre-industrial run) has been run. Focusing on the central North Atlantic, the difference between the SST_{MODEL} and SST_{TARGET} has revealed that the temperature-only restoring was not properly working since SST_{MODEL} tends very slowly to SST_{TARGET} at the

beginning of the simulation to diverge from the 7th year on (Figure 2.2a, Figure 2.3a). To counterbalance the additional flux term introduced by SST restoring during the simulations, sea surface salinity (SSS) is also restored to the preindustrial-run climatology. The SSS relaxation is used to avoid the progressive alteration of the mean ocean circulation and thermodynamical balance, reducing at least as possible the density anomaly. SSS restoring can be considered as a flux correction on freshwater fluxes which has no physical meaning. As for the SST, a flux formulation is used to restore SSS adding a feedback term in the freshwater budget to the freshwater flux *EMP*:

$$EMP = EMP^0 + \gamma_S \frac{(SSS_{MODEL} - SSS_{TARGET})}{SSS_{MODEL}}$$

where:

- *EMP* is the resulting freshwater flux (evaporation minus precipitation).
- SSS_{TARGET} is the climatological SSS for both the AMV phases.
- SSS_{MODEL} is the model SSS.
- γ_S is the negative SSS restoring term which indicates the magnitude of the damping in the salinity. Unit is mm/d.

Given the model-dependence nature of γ_S, a tuning of salinity damping term has been necessary to assess the best value which contributes to perturb the least possible the climate-system equilibrium. A range of γ_S has been tested on the mini-ensemble, varying from –27.70 mm/d to –864.00 mm/d with a τ_R from 5 years to 2 months for a 50-m MLD (Table 2.1). According to hfcorr diagnostics, setting γ_S equal to –432.00 mm/d ($\tau_R \cong$ 4 months for a 50-m MLD) determines a better restoring in terms of SST convergence towards the observed AMV phase (Figure 2.2b, Figure 2.3b), without

excessively altering the ocean circulation and preserving the characteristics of the water masses.

	#1	#2	#3	#4	#5
γ_S[mm/d]	-27.70	-166.67	-240.38	-432.00	-864.00
τ_R [d] (50-m MLD)	1805	300	208	116	58

Table 2.1. Salinity damping coefficients and relaxation time-scale, considering a 50-m Mixed Layer Depth, used in the sensitivity tests to estimate the best γ_S.

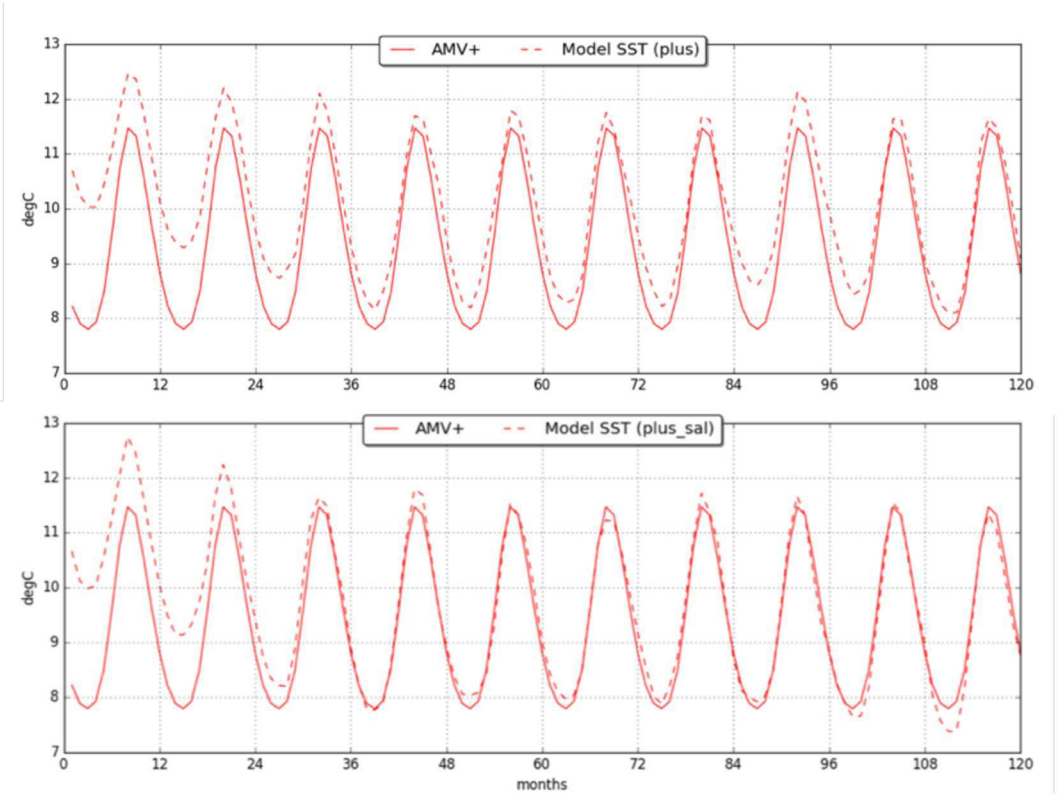

Figure 2.2. Central North Atlantic mean of SST_{MODEL} (dotted line) and SST_{TARGET} (solid line) before (top row) and after (bottom row) the implementation of salinity restoring of one member of the mini-ensemble during the simulated positive phase. For SST_{MODEL} ensemble mean values are shown.

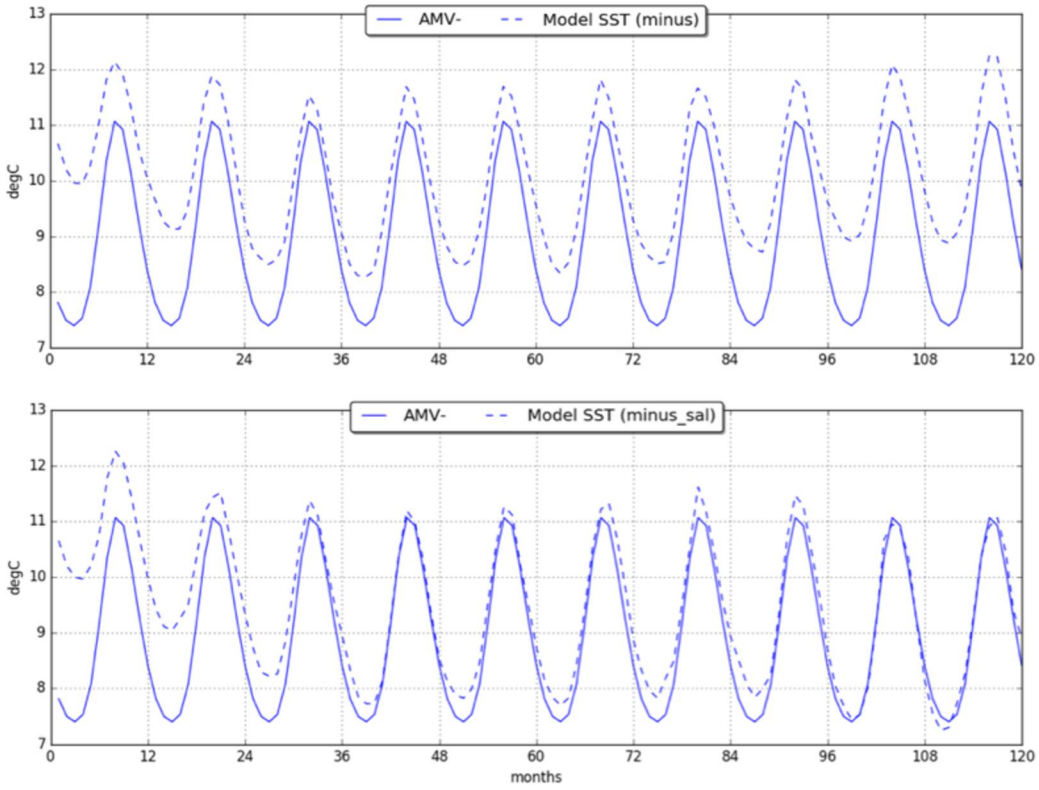

Figure 2.3. Same as the Figure 2.2 but for the negative phase

The SST/SSS restoring is applied over the North Atlantic (from 10°N to 65°N) based on a mask provided by DCPP protocol on a 2-degree horizontal grid. Outside this target region, the model is allowed to freely evolve. Following the protocol [Boer et al. 2016], the original AMV mask is extrapolated over land to minimize the interpolation errors and, using a bilinear method, is regridded onto the ORCA1 tripolar grid of NEMO ocean model (Figure 2.4). An 8-degree wide buffer zone is opportunely designed at the edge of the nudging area to minimize shocks and to avoid instabilities in the no-restoring region. Where the mask equals 1, a full nudging is applied. Fractional values allow a gradual reduction of the restoring rate, with a smooth transition from the full-nudging

region to a freely evolving region. Further ad-hoc corrections are made in some critical areas, such as along the coasts and where the Atlantic is linked to other basins: the Hudson strait in the Labrador Sea, the Danish strait in the Baltic Sea and the Gibraltar strait in the Mediterranean Sea. Using a flux formulation restoring the mask is directly applied on the flux term to prevent spurious values along the buffer zones. The mask is implemented in NEMO code as follows:

$$Q_{ns} = Q_{ns}^{0} + \frac{dQ}{dT}(SST_{model} - SST_{Obs}) * R_{Mask}$$

where R_{Mask} is a two-dimensional field.

To reduce the non-linear uncertainty related to the internal variability of the climate system, an ensemble approach is used. The DCPP protocol recommends to generate the ensemble using at least 25 "macro-perturbations" [Hawkins et al. 2016], i.e. considering 25 different ocean states as initial condition of each realization, in addition to only different atmospheric states ("micro-perturbation"). This ensures a better spread among the ensemble members. In this study, 32 members are considered taken from a multicentury pre-industrial run.

Two sets of idealized experiments have been performed where the perturbation via restoring is applied:

- *AMV+ experiments*: North Atlantic (10°N – 65°N) SSTs are restored to positive time-independent AMV anomaly (i.e. +1 standard deviation of the AMV index) superimposed on 12-month model climatology. No restoring is performed where the sea ice fraction is greater than 15%, which is the Sea-Ice Extent definition.

- *AMV- experiments*: they are analogous to AMV+ experiments, but it is considered the negative AMV anomaly (i.e. -1 standard deviation of the AMV index).

Each simulation is integrated over a 10-year period, allowing to catch the climate response to the AMV input, while longer simulations may lead to the aforementioned drift, introduced by the experimental setup [Ruprich-Robert et al. 2017].

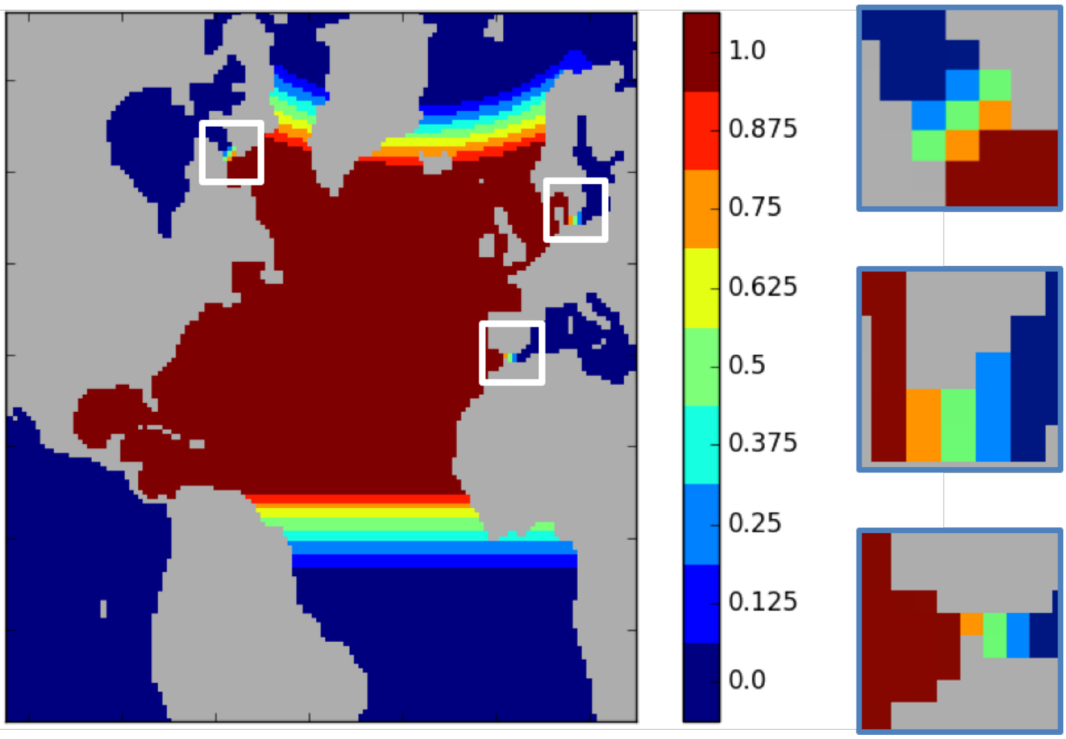

Figure 2.4: (left) Mask used to restore the SST in the North Atlantic on ORCA1 tripolar grid and (white squares in the left panel; magnified on the right panels) the critical buffer areas: (top) the Hudson strait in the Labrador Sea, (mid) the Danish strait in the Baltic Sea and (bottom) the Gibraltar strait in the Mediterranean Sea. The buffer zone increases with a step of 0.125 per latitude degree from zero (no restoring) to one (full restoring).

3 – Global climate impact of the AMV

3.1 Introduction

In this chapter, the global climate impacts of the AMV anomalies are presented. These are diagnosed in terms of difference patterns between the AMV+ and AMV- ensemble means, calculated for different key variables, to get the linear response of the climate system [Ruprich-Robert et al. 2017]. Last 8 years of each experiment have been considered – i.e. neglecting the first 2 years of simulation – allowing to the SST to converge towards the imposed pattern and obtaining a response biased by the initial conditions as little as possible. The statistical robustness of the results is evaluated by means of a two-tailed Student's t test, with a 95% confidence level of significance. Both summer and winter responses are analyzed so as to characterize the seasonal dependency of the AMV impact [García-Serrano and Doblas-Reyes 2012].

In order to put the CMCC model results in a broader context and also to characterize model-to-model uncertainties, a comparison with a similar set of DCPP experiments (40 members), performed with the CNRM-CM5 climate model [Voldoire et al. 2013, and reference therein] is presented. This comparison is part of a scientific collaboration established with the CERFACS (Centre Européen de Recherche et de Formation Avancée en Calcul Scientifique) research group in Toulouse (France). The CNRM-CM5 model used to perform the experiments has been jointly developed by CERFACS and CNRM-GAME (Centre National de Recherches Météorologiques – Groupe d'étude de l'Atmosphère Météorologique). The CNRM-CM5 model is based on the following components. For the atmosphere, the ARPEGE-Climate model (Community Action de Recherche Petite Echelle Grande Echelle) version 5.2 is used, characterized by a Gaussian grid with 1.4° horizontal resolution and 31 vertical levels

with a progressive hybrid pressure discretization. The ocean component is NEMO version 3.2, a previous release to the one used in CMCC-CM2-SR5 with which shares the same horizontal grid, 1° ORCA tripolar grid, but differs in vertical resolution (42 levels versus the 50 vertical levels of CMCC model). The GELATO5 (Global Experimental Leads and ice for ATmosphere and Ocean version 5) sea ice model is directly embedded in the ocean component of CNRM-CM5 and uses the same horizontal grid. SURFEX (Surface Externalisée) manages three surface schemes which represent the surfaces of natural land, inland water (lakes) and sea/ocean areas while the TRIP (Total Runoff Integrating Pathways) simulates river routing and water discharge from rivers to the ocean. Differently from the CMCC experimental setup, restoring is applied only to SST, not to sea surface salinity, assessing that no drift occurs in CNRM-CM5 simulations [Tech. Note II, Boer et al 2016].

3.2 Boreal Summer (June-to-September) Response

Over the North Atlantic Ocean, both CMCC and CNRM models show 2-m temperature anomalies which are consistent with the imposed AMV pattern. These include a significant warming over the entire basin and local maxima (up to 0.5°C) placed in the SPG and along the Eastern tropical branch (Figure 3.1). The anomalies are not twice the observed AMV pattern because of the high frequency of the ocean-atmosphere coupling. In fact, at mid-latitude and in the subtropics, atmospheric forcings has a dominant role over the surface ocean [Deser and Timlin 1998]. Nevertheless, a decrease of the air-sea interaction frequency in a coupled framework leads to spurious drift and non-physical model adjustment. For this reason, the magnitude of the restoring feedback coefficient, recommended by the DCPP protocol, has been chosen in order to

do not strongly constrain the SSTs over the Atlantic, allowing to the climate system to freely evolve.

The Atlantic warming reverberates on the European region, with positive anomalies over the Iberian Peninsula, North-West Africa and Mediterranean basin, particularly pronounced and significant over the whole continent in the CMCC model [Sutton and Hodson 2005, Sutton and Dong 2012, Knight et al. 2006, Mariotti and Dell'Aquila 2012]. On the other side of the Atlantic, both models show a zonal dipole over Canada, with cold (warm) anomalies over the Pacific coasts (the Ontario region) [Wang et al. 2012]. A positive AMV leads to warmer temperatures over Central America, South-Western U.S. and North-East Brazil, consistent with the observations [Sutton and Hodson 2005, Knight et al. 2006]. The models are able to reproduce the AMV-related linkages, not only in the surrounding areas of the Atlantic. The North Pacific Ocean exhibits warm anomalies in the interior and cool anomalies along the North American coast, closely resembling the negative phase of the Pacific Decadal Oscillation (PDO) [Mantua and Hare 2002]. A slight but significant warming (0.1 – 0.2°C) affects the West Tropical Pacific (WTP), the Maritime continent and the Northern part of Indian Ocean, in agreement with the existing literature [Kucharski et al. 2016a, Kucharski et al. 2016b, Zanchettin et al. 2016, Sun et al. 2017]. A common prominent maximum is evident over Mongolia even if the adjacent Russian region shows significant but opposite response in CMCC and CNRM models. In the CMCC (CNRM) model, the latter signal could be associated with meridional advection of warm (cold) air flowing from the Arctic Ocean sector to Eurasia [Komatsu et al. 2018], with an increase of the fresh water inflow from the Siberian rivers. Nevertheless, further analysis is required to understand the mechanism behind this response. Other discrepancies between the two models, are evident, especially in the Southern Ocean.

Changes in atmospheric circulation are characterized by negative sea level pressure (SLP) anomalies which involve the most part of the Northern Hemisphere with minima centered in the Nordic Seas, Baffin Bay and North Atlantic Ocean (Figure 3.2). In the whole North Pacific, the increased SLP is the signature of the mass compensation of the reduced North Atlantic SLP, suggesting that a warm phase of the AMV can alter the Walker circulation [McGregor et al. 2014, Li et al 2016, Ruprich-Robert et al. 2017]. A closer inspection aiming to better understand how this teleconnection affects the global climate is given in chapter 5. Unlike the CMCC model, CNRM model shows high and significant negative values also over the whole Antarctica.

Marked changes in precipitation field are evident along the tropics in both the models, with positive anomalies straddling most of the tropical belt (Figure 3.3). These anomalies are consistent with a northward shift of the Inter-Tropical Convergence Zone (ITCZ) because of an inter-hemispheric energy imbalance given by the North Atlantic warming which in turn modifies the Walker circulation [Donohoe et al. 2014, Ruprich-Robert et al. 2017]. The displacement is clearer in CMCC experiments compared to CNRM one in which just a reinforcement of the northern side of the ITCZ is noticeable. This result corroborates the idea of the ITCZ-shift positive feedback, as described by Wang [2012] and in section 1.3 of this thesis, that leads to an increase of rainfall over the semiarid Sahel region, with human and socio-economic impacts. On the Eastern side of the Pacific Ocean, the Maritime continent experiences enhanced rainfall with anomalies suggesting a South-Westward shift of the South Pacific Convergence Zone (SPCZ), a band of low-level convergence, cloudiness and precipitation. This also leads wetter conditions over Indian peninsula conferring a role for the AMV in modulating the Indian Summer Monsoon (ISM) rainfall, only in CMCC model [Goswami et al. 2006, Krishnamurthy and Krishnamurthy 2016, Ruprich-Robert et al. 2017]. The CNRM model exhibits a noisy pattern and may reflect the incapacity of the model to reproduce

multidecadal Indian observed precipitation [Joshi and Ha 2018]. Significant reduced rainfalls affect, off the equator, the Central and Western Pacific, with localized minima over California and Amazonia region, while above-normal precipitation marginally involves the Baffin Bay and the Nordic Seas.

Interestingly, European sector shows a different model-to-model response among the analyzed variables. The CMCC model shows a reduction of SLP, consistent with significant warm and dry anomalies, which is partially in line with previous studies [Sutton and Hodson 2005, Sutton and Dong 2012, Ruprich-Robert et al. 2017], even if no precipitation occurs over the entire continent in AMV experiments. By contrast, more uncertainty emerges in CNRM simulations, in which non-significant response dominates the Central Europe.

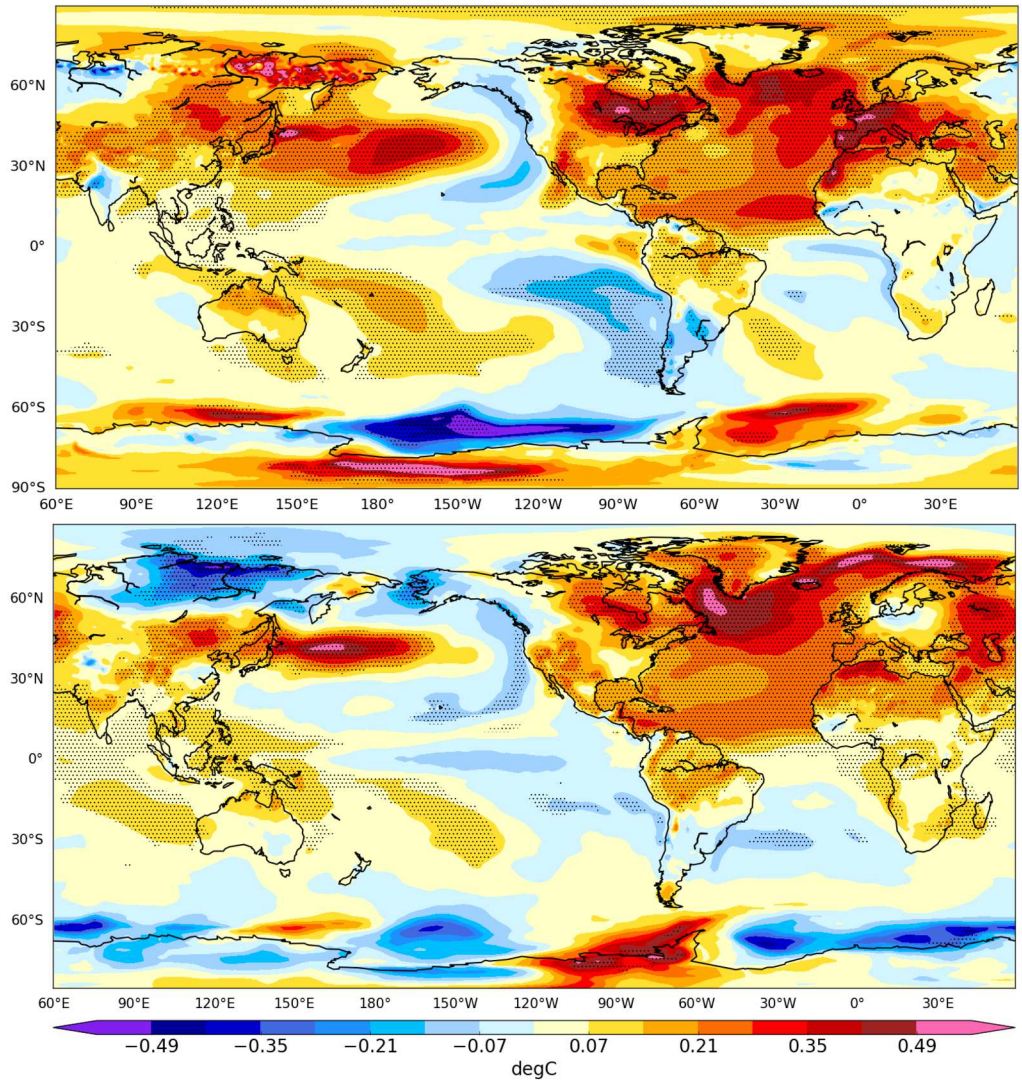

Figure 3.1 Boreal summer (JJAS) differences between the last 8-year ensemble mean of the positive and negative phases of the AMV experiments for 2-m temperature in CMCC (top panel) and CNRM models (bottom panel). Dotted regions display significant values (Student's t test with 95% confidence level)

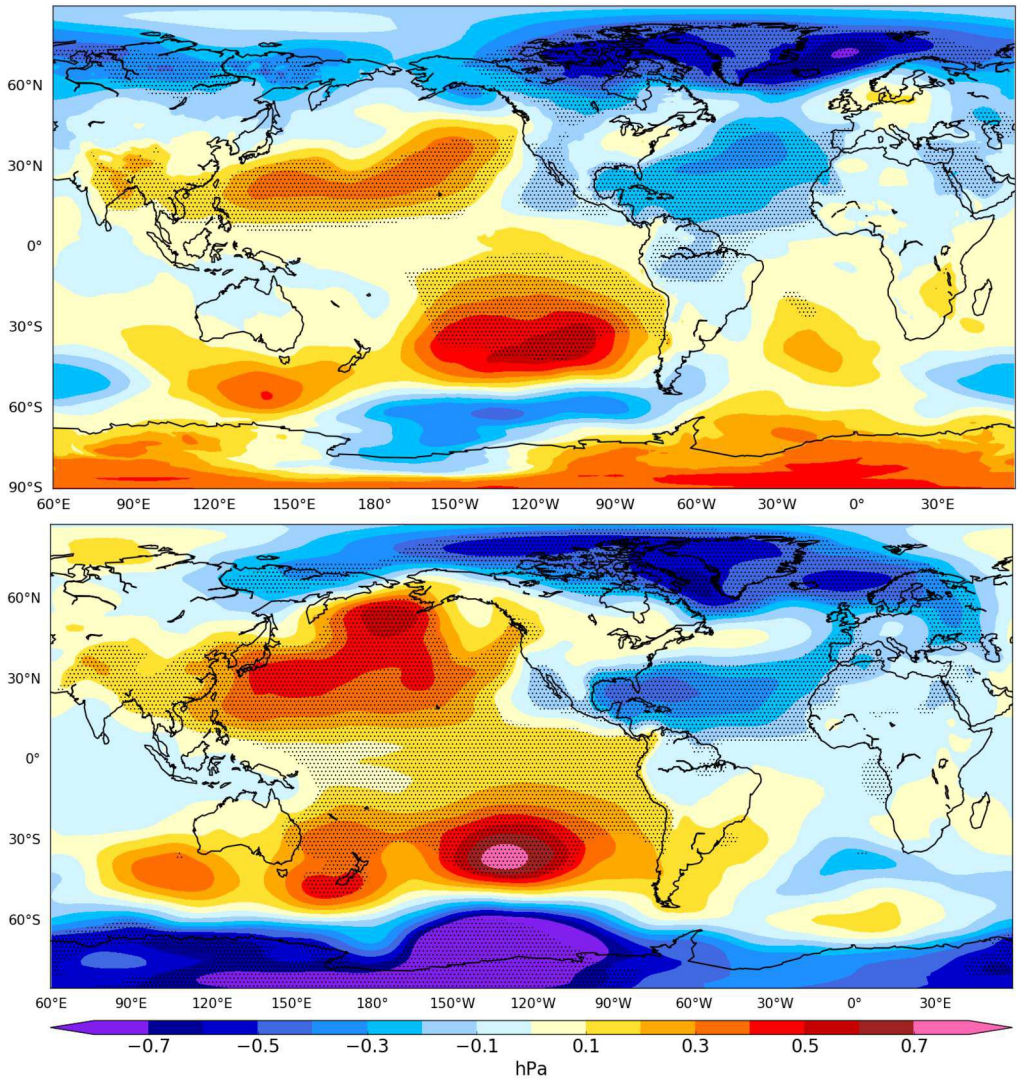

Figure 3.2. As in Figure 3.1, but for sea level pressure.

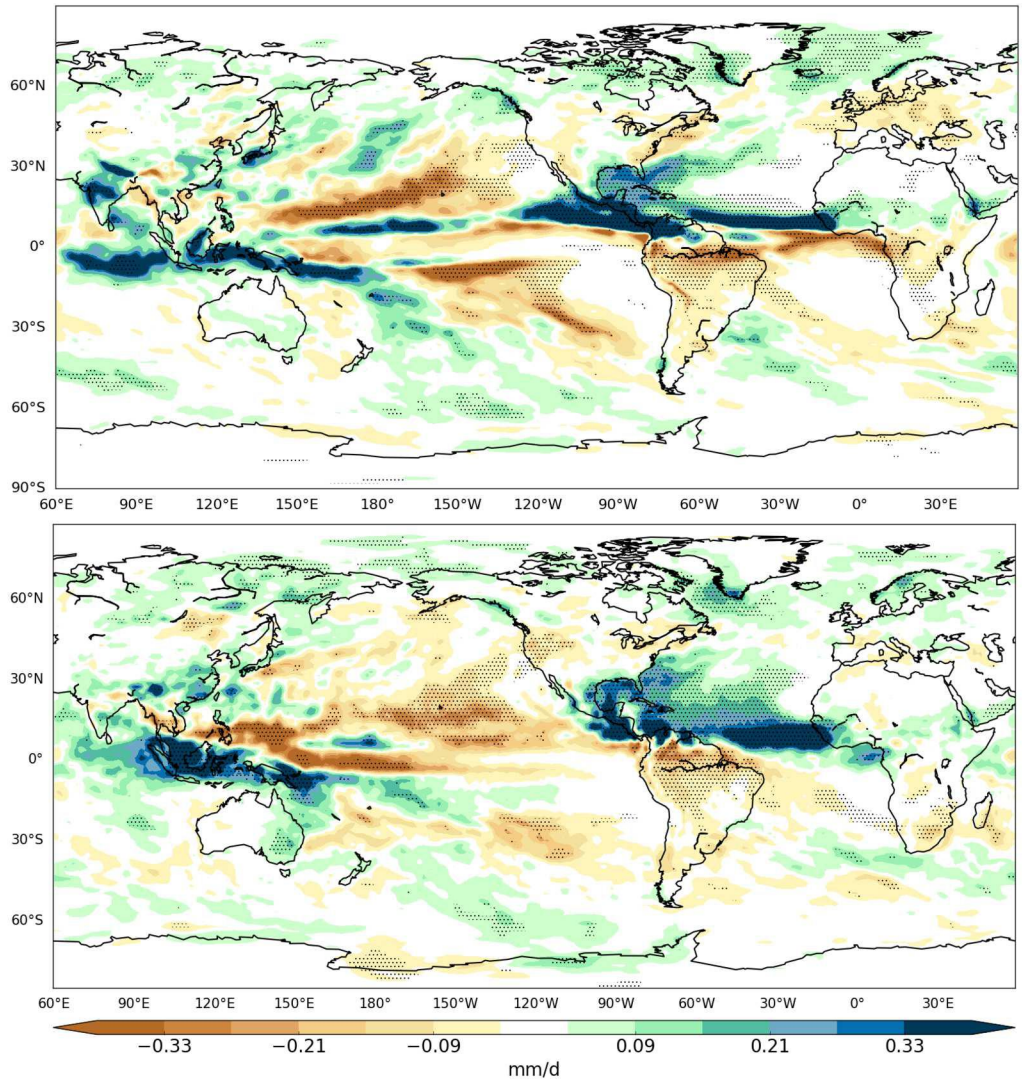

Figure 3.3. As in Figure 3.1, but for precipitation.

3.3 Boreal Winter (December-to-March) Response

During Boreal winter, the 2-m temperature response to fixed SST anomalies resembles the AMV pattern over the North Atlantic even if, mostly in CNRM model, the signal is less significant on the Western side of the basin (Figure 3.4) which is collocated along the Gulf Stream. This means that the high heat transport from lower latitudes due to the fast current and the variability of the system is greater than the imposed SST anomalies. Nevertheless, the main features of the AMV are well reproduced over the Atlantic Ocean, including both the maxima over the SPG and Eastern Tropical Atlantic. Significant warming affects Central America, Tibetan plateau and the Saharan region, with maxima over the Middle East and Indian sub-continent (~0.4°C). The North Pacific Ocean is reminiscent of the IPO-like response, as estimated in DCPP protocol (Figure 3.5), especially in CMCC model where the structure of the negative signal is not interrupted by anomalies of the opposite sign [Sutton and Hodson 2006, Ting et al. 2011, Barcikowska et al. 2017]. The models disagree over the Bering Strait region where the CNRM model presents a cold air anomaly up to the Pacific-side of the Siberian region. Positive anomalies characterize also the WTP, Maritime continent and the Indian Ocean, similar to Boreal summer response, reinforcing the idea that such feature is fed by the positive AMV phase. The Arctic Ocean response reveals a significant increase of air temperature, consistently with existing literature [e.g. Miles et al. 2014], that results in thinner sea ice pack that is more prone to melt, leading to a smaller sea-ice cover at the end of the melting season. Substantial discrepancies between the two models are evident over the Euro-Mediterranean sector, where the AMV induces opposite patterns, although it is worth noting that only the CMCC model shows significant variability over the Mediterranean region.

The SLP anomaly field can be considered a proxy of the atmospheric flow changes and provides a measure of the alteration of the large-scale surface circulation induced by the polarities of the AMV. Both models feature a broad-scale negative SLP anomaly over the tropical Atlantic, as a likely consequence of the tropical Atlantic AMV-related warming (Figure 3.6). Nevertheless, there are very few communalities on the global scale. Model-to-model dissimilarities during Boreal winter are partly linked to the efficiency of the restoring, especially over the SPG, representing a deep-water formation site. Seawater at the surface of the ocean is intensely cooled by the wind and surface air temperatures. Wind flowing over the water also produces a great deal of evaporation, resulting in an increase in the sea salinity and so in the water-mass density along with the temperature decrease. This process is obviously stronger during the colder season, leading to a deepening of the mixed layer compared to the summer since the imposed SST is vertically distributed over a great depth. Thus, it is not so unexpected that the model diverges in this season due to a less effective SST restoring. In CMCC, the SLP response shows a meridional significant dipole, with a positive lobe over Greenland and a negative one over Central Europe extending over the Atlantic, associated with a statistically-significant precipitation increase (Figure 3.7). This pattern bears some resemblance with the negative phase of the NAO, in agreement also with 2-m temperature field, even though only a slight SLP weakening occurs at the Azores High. To corroborate these claims, the geopotential height at 500 hPa (hereafter Z500) is analyzed (Figure 3.8, color shading). The winter response shows significant positive anomalies over the Azores in contrast with the SLP field. A portion of the reversed signal could be explained by the meridional gradient of temperature which basically drives the north-south dynamics. Hence, the zonal mean of Z500 is subtracted from its full field in order to disentangle the dynamic from the thermodynamic response. According to the departure from the zonal average of the Z500 (hereafter Z500*), the

AMV warming does not project onto a negative NAO since there are two maxima, one over Greenland and one over Azores (Figure 3.8, contours). In CNRM, the European SLP minimum is shifted southwards compared to the CMCC, consistently with its precipitation anomaly, while a non-significant maximum is stretched from Scandinavia to British Islands and beyond. The Z500 diagnostics reveals a reminiscence of the negative phase of the East Atlantic Pattern (EAP-) [Barnston and Livezey 1987]. The EAP is the second prominent mode of low-frequency variability over the North Atlantic and consists of a north-south dipole spanning the North Atlantic from east to west. The anomaly centers of the EAP are displaced southeastward to the approximate nodal lines of the NAO pattern. For this reason, the EAP is often interpreted as a southward-shifted NAO pattern. The EAP- is borne out by both the Z500* and the dry-wet pattern over Europe despite statistically irrelevant. Ruprich-Robert et al. [2017], following a similar experimental protocol, found comparable results using other two model frameworks: NCAR-CESM1 [Kay et al. 2015], which has the same atmospheric component of CMCC-CM2-SR5, and GFDL-CM2.1 [Delworth et al. 2006, Wittenberg et al. 2006]. This diversity in atmospheric responses highlights the relevance of the aforementioned model uncertainty in assessing the AMV impacts and the needs for a multi-model framework. Ruprich-Robert and co-workers also argued that the negative anomalies over Europe might depend on the winter reduction of the mean advection of air flowing from the Atlantic Ocean to continental Europe, associated to a decrease of the westerly winds.

In the North Pacific, the Aleutian low is weakened due to the positive SLP anomaly, even though this feature is poorly significant in CMCC (Figure 3.6). This positive anomaly allows the injection of cold air from the Arctic towards North-Western America, via a drop in the mean (cyclonic) advection [Ruprich-Robert et al. 2017]. The Z500 clearly project onto the negative phase of the Pacific-North America (PNA)

climate mode, reflecting a two-dipole pattern, with anomalies of similar sign located over the Aleutian Islands and over the South-Eastern U.S. [Barnston and Livezey 1987]. Precipitation changes along with SLP indeed project the entire Pacific Ocean onto the cold phase of the El Niño–Southern Oscillation (ENSO) [Trenberth et al. 1998, Kucharski et al. 2011]. The Eastern Pacific is characterized by an increase of SLP, compensated by the negative anomalies of the Indian and Western-Pacific Ocean, resembling the IPO in its negative polarity [Zhang and Delworth 2015]. Anomalous cyclonic circulation over the WTP is consistent with the recent findings of Sun et al. [2017] which attribute this below-average SLP to a weakening of subtropical North Pacific westerlies and a strengthening of the Wind-Evaporation-SST (WES) mechanism (for further details, see Chapter 5). A positive SLP anomaly is localized over South-Western U.S. with reduced rainfall in both the models (Figure 3.7). The AMV-induced temperature gradient shifts northward the Atlantic ITCZ, with enhanced rainfalls over North Brazil and equatorial Africa, while the SPCZ signal is quite noisy and not statistically relevant, with positive anomalies over the Maritime continent.

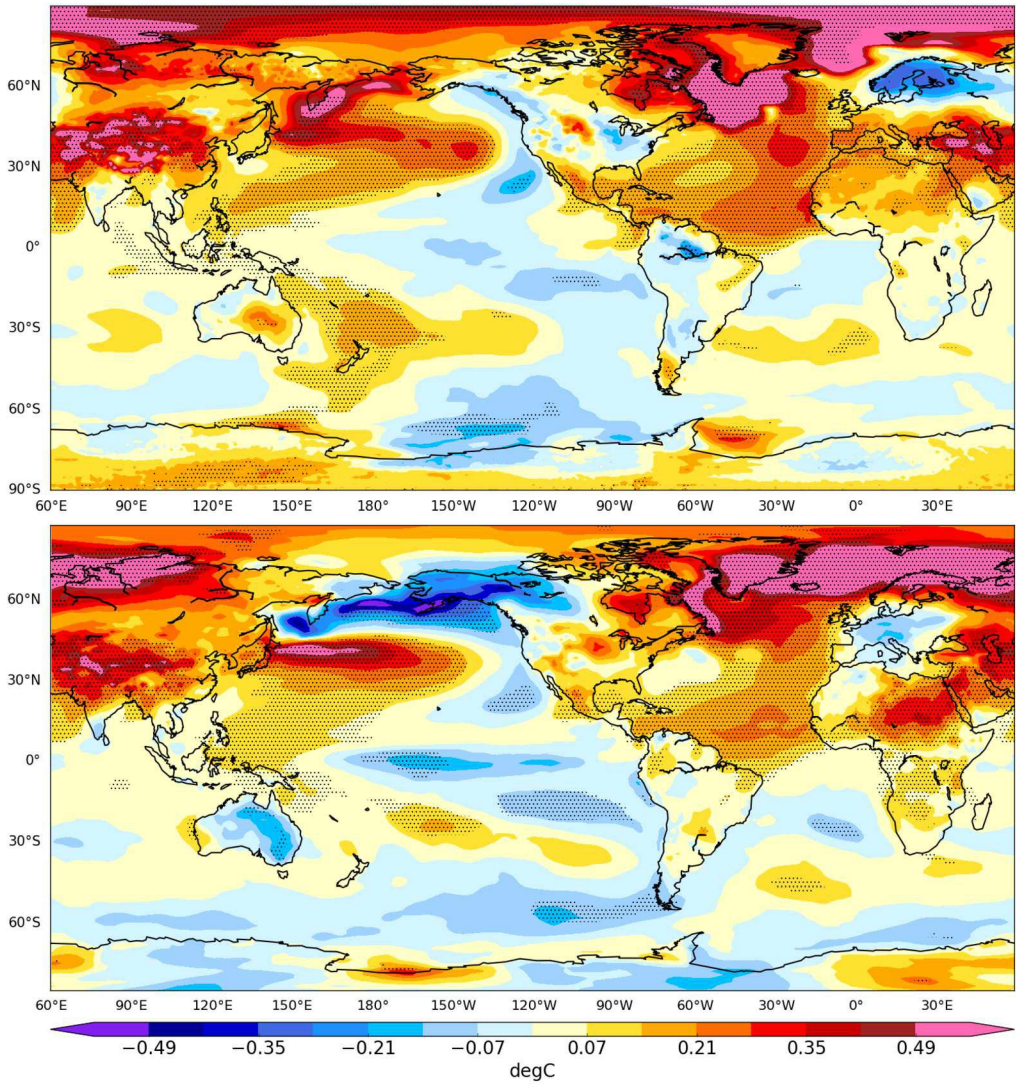

Figure 3.4. Boreal winter (DJFM) differences between the last 8-year ensemble mean of the positive and negative phases of the AMV experiments for 2-meter temperature in CMCC (top panel) and CNRM models (bottom panel). Dotted regions display significant values (Student's t test with 95% confidence level).

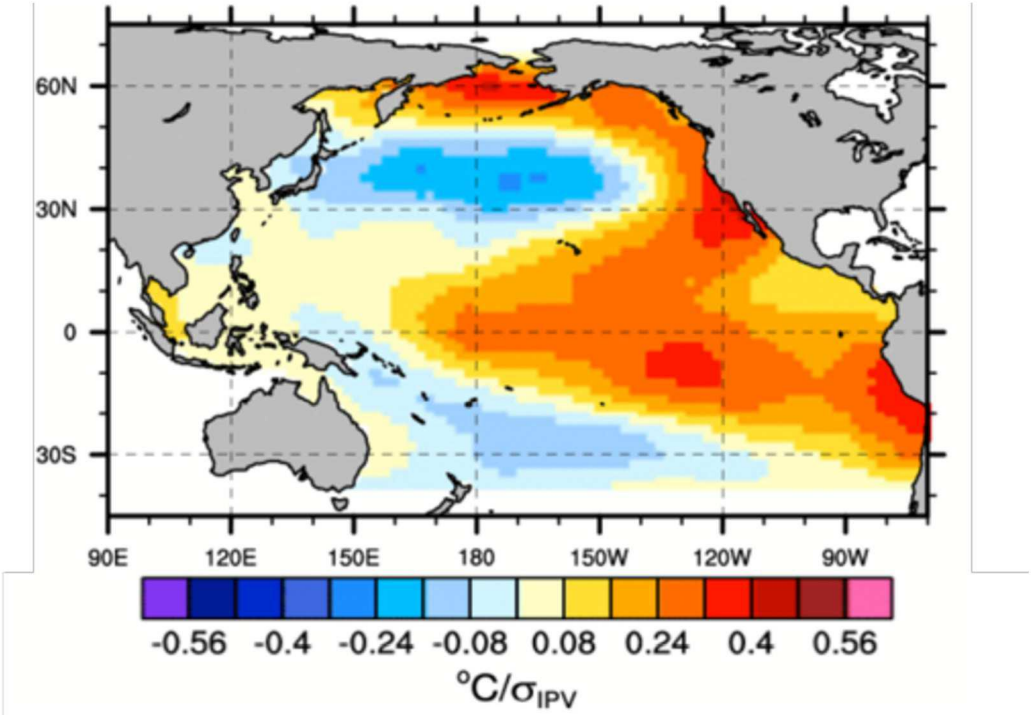

Figure 3.5. Interdecadal Pacific Variability SST anomalies (IPV) obtained from regression of ERSSTv4 annual residual SST (i.e. forced component removed) on the IPV time series. Figure from Tech. Note 1, Component C, Boer et al. 2016.

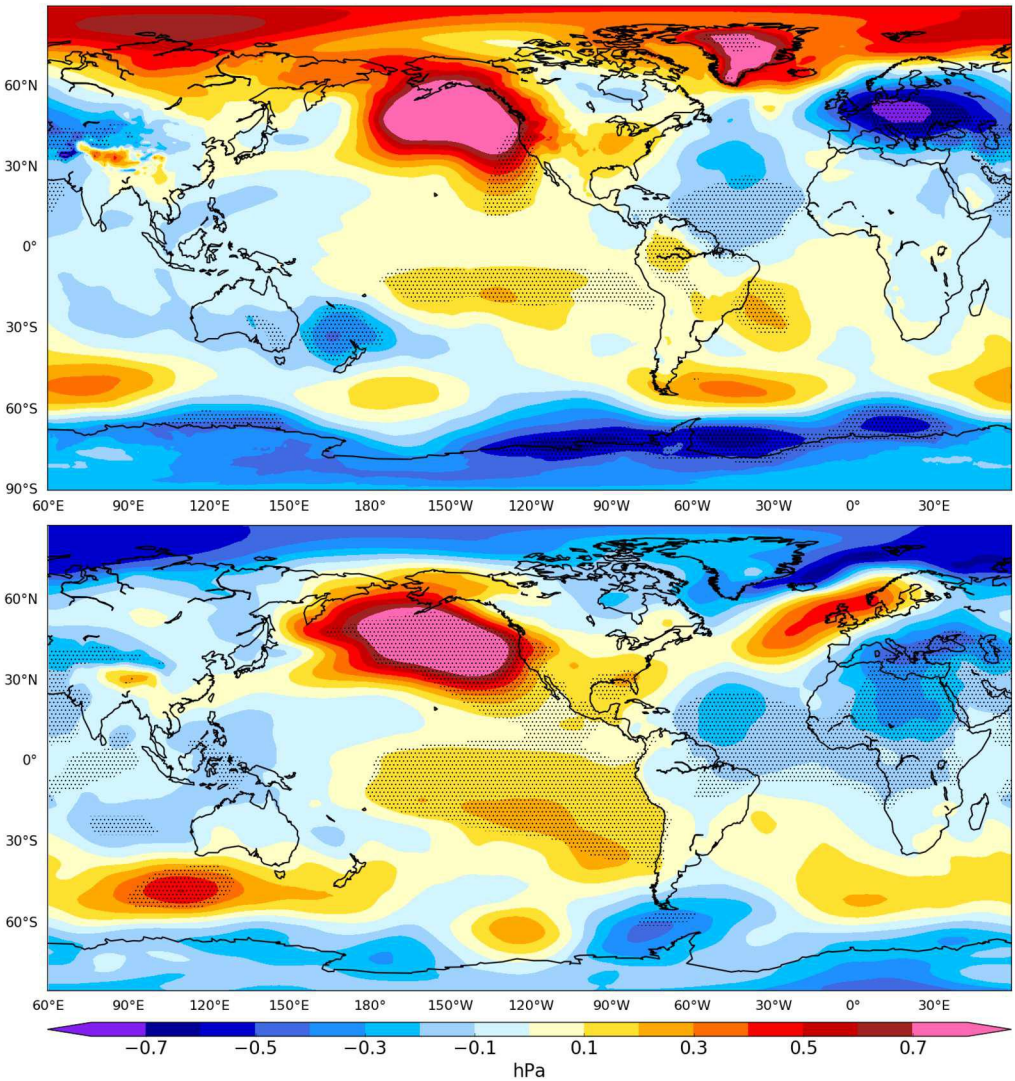

Figure 3.6. as in Figure 3.4, but for sea level pressure.

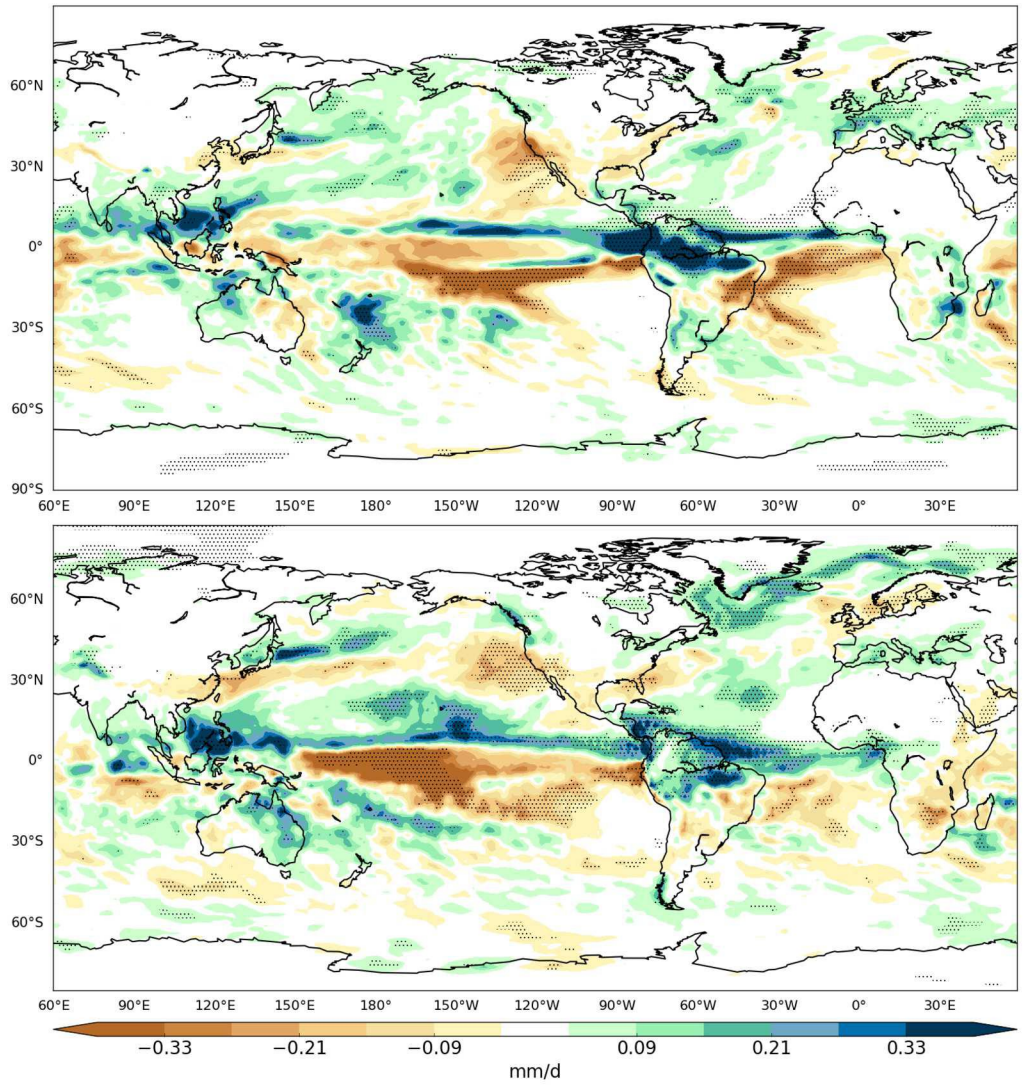

Figure 3.7. As in Figure 3.4, but for precipitation.

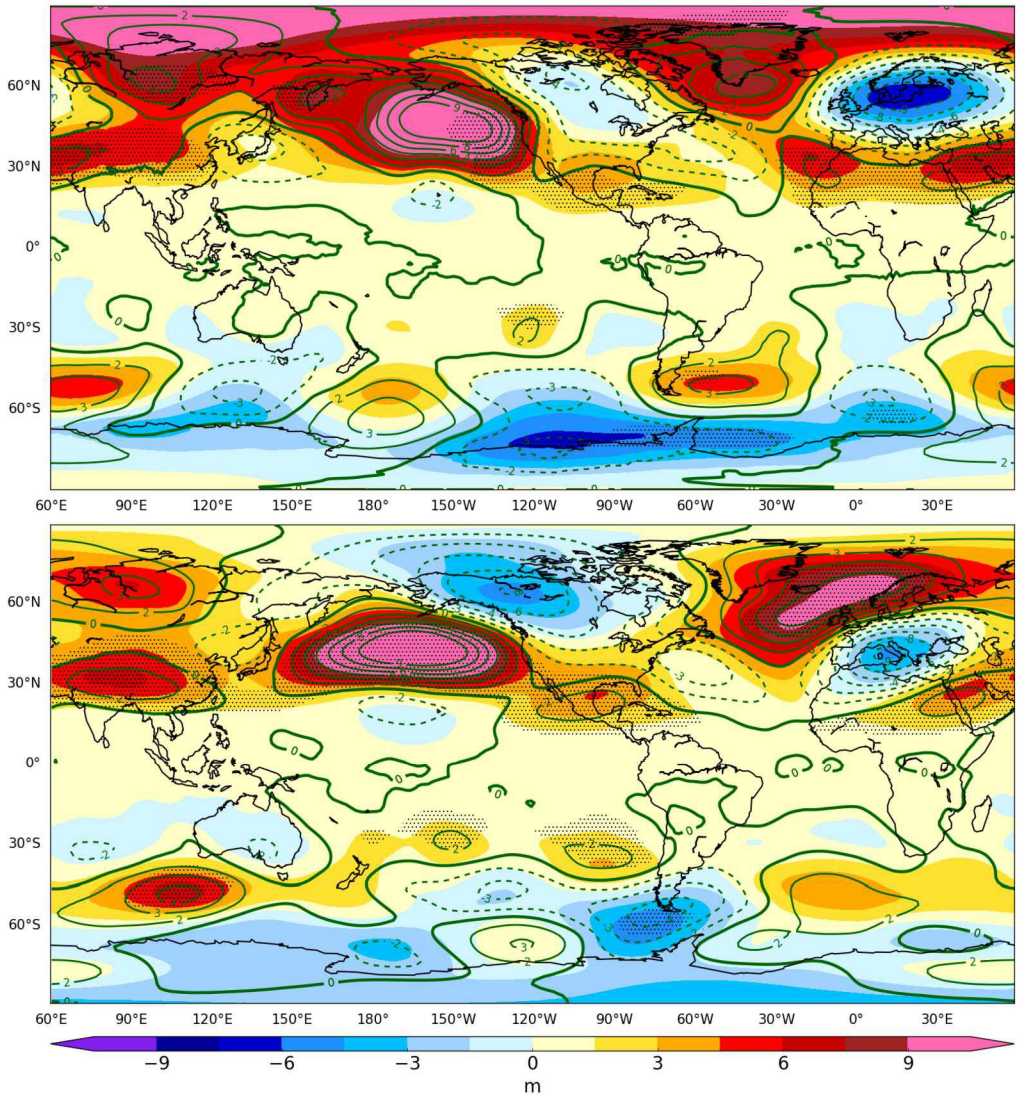

Figure 3.8. As in Figure 3.4, but for geopotential height at 500-hPa (shading) and its departure from the zonal mean (contours; interval of 1.5 m).

3.4 Quantifying the AMV Impacts

The linear response of the AMV impacts, described in the previous sections, are evaluated as the difference between the ensemble means of the AMV+ and AMV- experiments and a two-tailed Student's t test has identified significant regions. Here, a different metrics is used to quantify the decadal strength of the AMV impacts, a signal-to-total-variance ratio (hereafter SNR). The method is based on a signal-to-noise ratio computed by Sutton and Hodson [2007] and later modified by Ruprich-Robert et al. [2017] for their analysis of AMV impact experiments. Unlike the t test, the SNR provides a useful, physically relevant, measure of the predictability in terms of decadal variance.

The signal S is the inter-ensemble variance and is computed as follows:

$$S = \left(\frac{AMV_{plus} - AMV_{minus}}{2}\right)^2,$$

where

$$AMV_{plus} = \frac{1}{n/2}\sum_{i=1}^{n/2}(x_i^+)$$

$$AMV_{minus} = \frac{1}{n/2}\sum_{i=1}^{n/2}(x_i^-)$$

the variable x^+ *(*x^-*)* represents the 8-year average of the target field (e.g. SLP) in each member of the AMV+ (AMV-) experiments; *n/2* is the number of the members in each experiment (i.e. 32 members), and the noise N is sum of the inter-ensemble and intra-ensemble variances and is computed as follows:

$$N = \frac{1}{n-1}\left[\sum_{i=1}^{n/2}(x_i^+ - X)^2 + \sum_{i=1}^{n/2}(x_i^- - X)^2\right]$$

where X represents the average of the two ensemble means and is equal to:

$$X = \frac{AMV_{plus} + AMV_{minus}}{2}$$

Thus, the SNR is a variance ratio of S and N, and can vary from zero (i.e. no signal due to the AMV) to one (i.e. all the variability is explained by the difference of the AMV polarities). Under the hypothesis of complete predictability of the AMV, the SNR indicates the percentage of the predictable variance of the decadal variability and, in this context, can reflect the upper threshold of predictability due to the AMV impact. For instance: for a SNR of 30% associated with a decadal variance of 1°C^2, the AMV accounts for 0.55°C (i.e. $\sqrt{0.3} \times \sqrt{1}$) of the 1°C anomaly. It is important underline that this method is not aimed to quantify the AMV predictability, but only the variability forced by the phenomenon.

The SNR of 2-m temperature field for boreal summer shows, as expected, high values over the North Atlantic, since that is where SSTs are restored to the AMV anomalies (Figure 3.9). Relatively large SNR values are also evident over Western Europe, Mediterranean basin and surrounding regions for both models (up to 35%), highlighting a role for the AMV in explaining the decadal variability over those regions. For North America, the SNR values over California and Great Lakes regions are consistent with both the simulated and the observed AMV response patterns [Enfield et al 2001, McCabe et al. 2004, Wang et al. 2018]. Marked predictability covers the WTP and the warm anomalies of the negative PDO-like signal (Pacific Decadal Oscillation signal), encouraging the hypothesis of a teleconnection between the main

oceanic basins. Large predictability emerges also from the North-East Brazil in terms of 2-m temperature and precipitation, coherent with their respective anomalies. This reinforces the involvement of the AMV in decadal warm and dry periods over Amazonia [Knight et al. 2006, Ting et al. 2011].

Boreal winter response shows less predictability than the summer one since the DJFM season is characterized by more dynamic atmospheric flows. SNR of 2-m temperature reveals a lack of predictability along the Gulf Stream in both the models (Figure 3.10). In CNRM, the Labrador Sea experiences low values because of the deeper ocean convection during wintertime while CMCC simulations prevent the dilution of the imposed SST by restoring also the sea surface salinity. The WTP and the Kuroshio-Oyashio extension resembles the 2-m temperature summer SNR, showing great predictability which persists throughout the year. Over land, Sahel and Middle-East impact are well predicted and consistent with the other fields in CMCC and in CNRM, respectively.

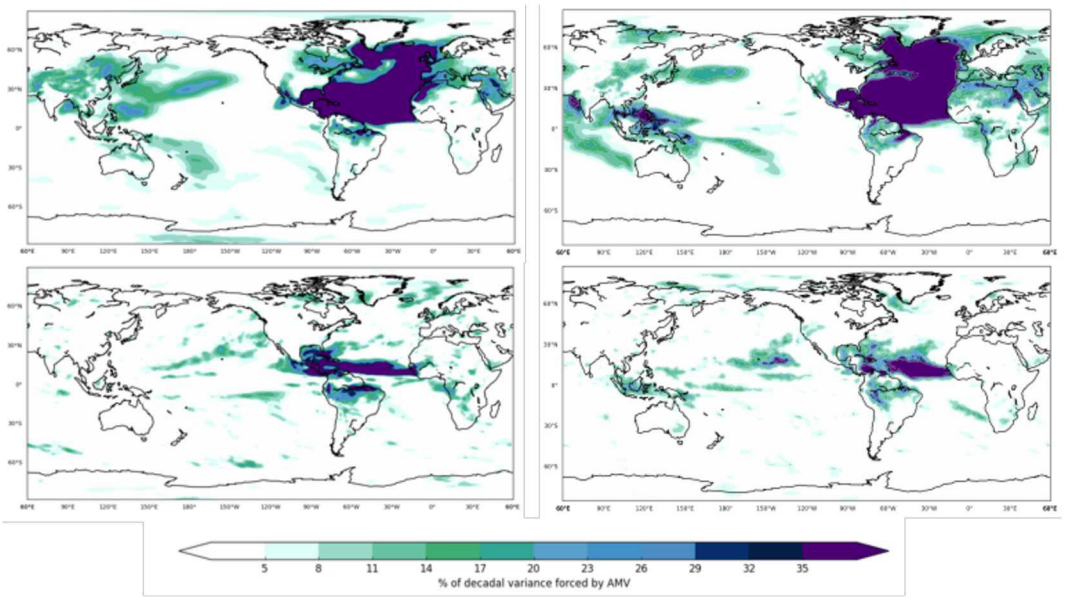

Figure 3.9. Boreal summer signal-to-total-variance ratio for 2-meter temperature (top panel) and precipitation (bottom panel) in CMCC (left column) and CNRM models (right column).

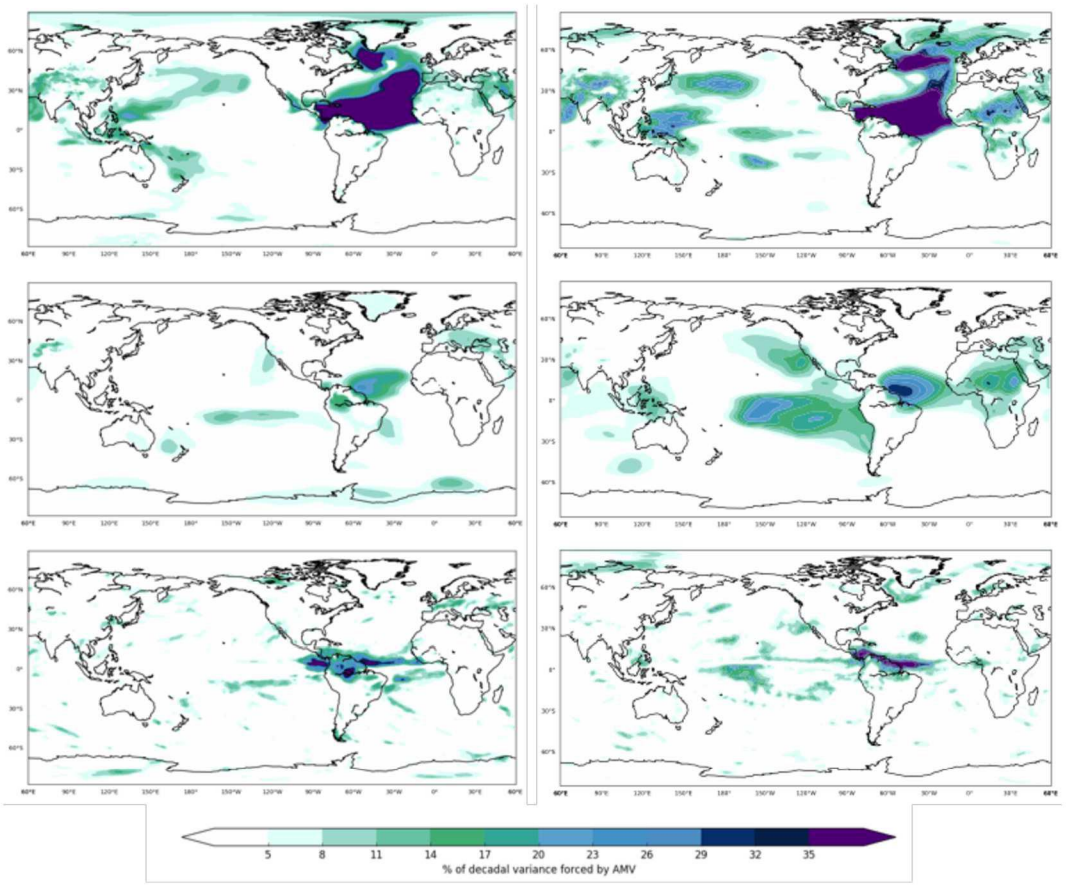

Figure 3.10. Boreal winter signal-to-total-variance ratio for 2-meter temperature (top panel), sea level pressure (middle panel) and precipitation (bottom panel) in CMCC (left column) and CNRM models (right column).

4 – Eddy-driven jet latitude variability on decadal time scales

In chapter 3 it has been shown how the boreal winter response features a significant variability in terms of sea level pressure, conferring a role to the AMV in setting large-scale circulation changes. Furthermore, recent studies have proven that the North Atlantic tropospheric jet stream exhibits a different behavior on the decadal timescale compared to the shorter ones, as well as, different processes can contribute in driving it [Davini et al. 2015, Woollings et al. 2010a, Madonna et al. 2017, Woollings et al. 2018]. An interesting issue is how the state of the sea surface temperature associated to the AMV phase can drive the mean state and high-frequency variability of the North Atlantic Jet (NAJ) in winter.

4.1 The North Atlantic Jet in the European-climate context

The westerly jet streams characterized the mid-latitude atmospheric circulation as regions of high wind speeds (Figure 4.1a,d). Typically, the tropospheric jet stream can be thought of as divided into two components. The first one, namely subtropical jet, implies the transport of momentum and vorticity due to the upper branch of the Hadley circulation [e.g. Lee and Kim 2003]. The second one, namely eddy-driven jet, associated with vorticity and heat transport anomalies caused by synoptic or more generally transient eddies [e.g. Hoskins et al. 1983]. Both types of jets in principle are maintained by non-uniform solar heating which provide energy to both the Hadley cell in the tropics and the mid-latitude transient eddies. Thus, the seasonal cycle of equator-to-pole temperature gradient implies weaker jet streams during Boreal summer

compared to the winter time. The subpolar jet is driven by variations in the transient eddy forcing [Thompson et al. 2003, Vallis and Gerber 2008]. Furthermore, the diffluent flow makes the exit region of the Atlantic jet particularly conducive to transient wave-breaking and the associated forcing [Gerber and Vallis 2009].

The term 'storm track' indicates that region where the mid-latitude cyclones and anticyclones favorably occur. European climate is strongly affected by the storms which propagate across the Atlantic from the east coast of North America. Their existence is again due to the meridional contrast in solar heating which drives horizontal temperature gradients, thereby facilitating a baroclinic instability in the troposphere. Cyclones and anticyclones grow on this instability, converting available potential energy into eddy kinetic energy and, hence, playing a large part in the heat transport from the tropics towards the poles. In Figure 4.1b,e, Northern Hemisphere storm tracks are shown by means of the eddy kinetic energy field in the ERA-40 reanalysis [Uppala et al. 2005]. Near the surface, the transient eddy activity is concentrated over the ocean basins, in the Pacific and Atlantic storm tracks, where surface roughness is lowest. At upper levels, however, eddy activity continues across North America so that the two segments of the storm tracks are joined. This indicates the presence of transient Rossby wave packets propagating from the Pacific into the Atlantic, influencing the jet stream [e.g. Franzke et al. 2004] and, ultimately, dissipating their energy near Europe.

In the Atlantic, dominant westerly winds at the surface level are the signature of the midlatitude eddy-driven jet streams with significant impacts also from societal perspective. Largest changes in flow variability arise over the ocean basins where stronger eddy-driven jets occur [Blackmon, 1976]. Jet stream variability is mainly represented by most of the major extratropical teleconnection patterns [Wittman et al. 2005, Monahan and Fyfe 2006]. Over the North Atlantic, the North Atlantic Oscillation (NAO) has been the dominant component of variability during wintertime since the

positive and negative NAO can explain 46% of the daily variance occurred during in the 1950-2006 period [Hurrell and Deser 2010]. A negative (positive) NAO phase can lead to anomalously weak (strong) high-latitude westerlies and to a southward (northward) shift of the subpolar jet, storm track and weather systems in the North Atlantic sector [Hurrell et al. 2003]. The NAO variability is usually characterized by patterns of SLP or geopotential height fields, as well as by analysis of wind field [Athanasiadis et al. 2009, Woollings et al. 2010a]. The remaining variance of the North Atlantic is accounted for 29% by the "Blocking" pattern (a zonal dipole of SLP with the maximum over Scandinavia and the minimum over Greenland), and the 25% is explained by the Atlantic Ridge, featured by a strong anti-cyclonic ridge off Western Europe [Cassou et al. 2004]. The latter shows some resemblance with the East Atlantic Pattern (EAP), suggesting a role for the EAP in modulating atmospheric circulation in December-to-February season [Hurrell 1995, Thompson and Wallace 2001, Hurrell and Deser 2009].

The standard deviation of monthly mean streamfunction anomalies at 250 hPa is shown in Figure 4.1c,f for Boreal summer and winter. High variability is noticeable at the downstream ends of the Pacific and Atlantic storm tracks, where the eddy-driven jets dominate. Further upstream, the subtropical jets are very strong and this inhibits the eddy-driven jets [Nakamura and Sampe 2002, Lee and Kim 2003, Eichelberger and Hartmann 2007]. Blocking is also common in these areas [Tyrlis and Hoskins 2008], contributing to the high standard deviations.

In a wider framework, these maps (Figure 4.1) show that Western Europe presents one of the most variable climates of any land area in the Northern Hemisphere, in both the seasons. Europe is directly affected by variations in the jet stream, and these in turn have many different influences, such as the remote effects of El Niño–Southern Oscillation (ENSO) [e.g. Brönnimann 2007] and the Madden–Julian Oscillation [e.g.

Cassou 2008], decadal variations of the AMV [e.g. Davini et al. 2015] and changes in the stratosphere. This large number of linkages means not only that the climate of Europe is highly variable, but also that variability stems from a large number of sources.

The experimental configuration simplifies the problem due to complications arising from air-sea interaction on long time scales, since the SST are restored towards a fixed pattern and forcing the atmosphere above. The positive and negative phases of the AMV do not simply translate to obvious and simple perturbation to the temperature gradient in the Gulf Stream region (Figure 4.2). In this study, a different equator-to-pole temperature gradient at surface is prescribed, as a factor controlling a number of processes in the region, in particular the mean position of the jet and the energy conversion from the mean state to eddies. The modification of the gradient in the high baroclinicity region is also non-trivial due to the combination of the imposed profile and its implications for land-sea thermal contrast. Therefore, a targeted investigation in the AMV experiments can shed light on the decadal behavior of the NAJ position and, consequentially, on its impact over Europe.

4.2 Estimating the North Atlantic Jet speed and latitude indices

Different techniques are used to diagnose jet streams directly in the upper-level wind field [e.g. Barton and Ellis 2009]. Nevertheless, Woollings et al. [2010a] argued that the best characterization for the eddy-driven jets emerges from the lower-tropospheric zonal wind, allowing to disentangle the portion of the large-scale flow that is driven by transient baroclinic eddies. In fact, the effect of eddies on the mean flow is to decrease the vertical shear and to accelerate the barotropic westerly flow, mostly at lower levels [e.g. Hoskins et al. 1983]. The upper-level wind might also be partly

thermally driven, even in the North Atlantic sector [Li and Wettstein 2012]. Thus, the lower-level wind is considered best for diagnosing the variability of the eddy-driven jet [Madonna et al. 2017].

Jet speed and latitude have been computed following the method developed by Woollings et al [2010a] and subsequently modified [Woollings et al. 2014]. In each experiment, the speed and latitude of the eddy-driven jet stream is computed as follows:

1. The 850-hPa zonal wind at daily timescale is considered (hereafter U850).
2. U850 is zonally averaged over the North Atlantic (a sector delimited by 0° – 60°W and 15°N – 75°N) to obtain a meridional wind profile.
3. A 10-day Lanczos filter with a window of 61 days is used to further remove short time-scale noise.
4. Jet speed is computed as the maximum westerly wind speed of the resulting profile
5. Jet latitude variability is finally defined as the latitude at which this maximum is found.

The authors (i.e. Woollings et al. 2010a) have tested the algorithm under different conditions to verify its robustness. For instance, very similar results have been obtained also removing the seasonal cycle or not applying the low-pass filter while, on the contrary, jet speed and latitude are sensible to the choice of the longitudinal box.

4.3 The southward shift of the North Atlantic Jet in AMV experiments

Following the aforementioned approach, the Probability Density Function (PDF) of the latitude variability of the NAJ in both the AMV phases is assessed for CMCC model (Figure 4.3). Each complete winter (DJF) from the second year of each

realization of the ensemble contributes to the PDF. The fit curve has been drawn considering a standard smoothing parameter of $h = 1.06\sigma n^{-1/5}$, where σ is the standard deviation and n is the sample size. The distribution shows three clear preferred jet positions, highlighted by the maxima in occurrence and well separated by relative minima. The trimodality of the North Atlantic eddy-driven jet stream resembles the one computed by Woollings et al. [2010a] for ERA-40 reanalysis considering the historical period December 1957 – February 2002, even though the absolute maximum does not correspond (Figure 4.4). A trimodal structure reflects the existence of distinct flow regimes [Woollings et al. 2010a, Hannachi et al. 2012]. During a positive phase of the AMV, the NAJ shifts southwards during wintertime in fact the NAJ maximum speed occurs at lower latitudes. Looking at U850 (Figure 4.5, shaded areas), the displacement of the NAJ is more evident with anomalies of approximately 0.7 m/s. Consistent with the southward NAJ displacement, a decrease of the eddy heat transport is found (Figure 4.5, contours), due to the meridional SST gradient reduction nearby the North American eastern seaboard. As mentioned in the previous section, the eddy-driven jet can be also detected in the upper-level 200-hPa wind field (Figure 4.6) since the departure from the mean state is not confined to the lower level. Changes in the upper tropospheric wind field are diagnosed with the variance of the 9-day high-pass-filtered geopotential height at 500 hPa, a proxy of the atmospheric eddy activity (Figure 4.7). The analysis reveals a significant decrease of the eddy activity with the minimum centered over northern Europe from which one can speculate that the simulated NAJ shift arises downstream of the location thereof. In order to understand the process of baroclinic instability at stake, the Eady Growth Rate is used. This parameter provides an estimate of the timescale associated with the development of a synoptic-scale baroclinic wave. Following Hoskins and Valdes [1990], the local baroclinicity at 775 hPa (s) is computed as:

$$s = 0.31 \frac{f}{N} \frac{\partial u}{\partial Z}$$

where f is the parameter of the Coriolis force, N is the Brunt-Väisälä frequency, $\frac{\partial u}{\partial Z}$ is the vertical wind shear, u is the horizontal wind speed and Z is the vertical height. Interestingly, the Eady Growth Rate (Figure 4.8) decreases over North American east coast, at the same latitude where negative anomalies of the eddy heat flux are found (Figure 4.5). The storm track, therefore, moves southward, mainly due to the zonal wind shear, consistent with the reduction of the meridional SST gradient, as in the case of the positive phase of the AMV.

In terms of climatic impact, significant precipitation is found over Central Europe (Figure 4.9, shaded areas). Focusing on the velocity potential at 850 hPa, the lack of convergence structures corroborates the hypothesis that the rainfall shift over Europe is associated with a displacement of the eddy-driven jet, also supported by U850 field (Figure 4.5).

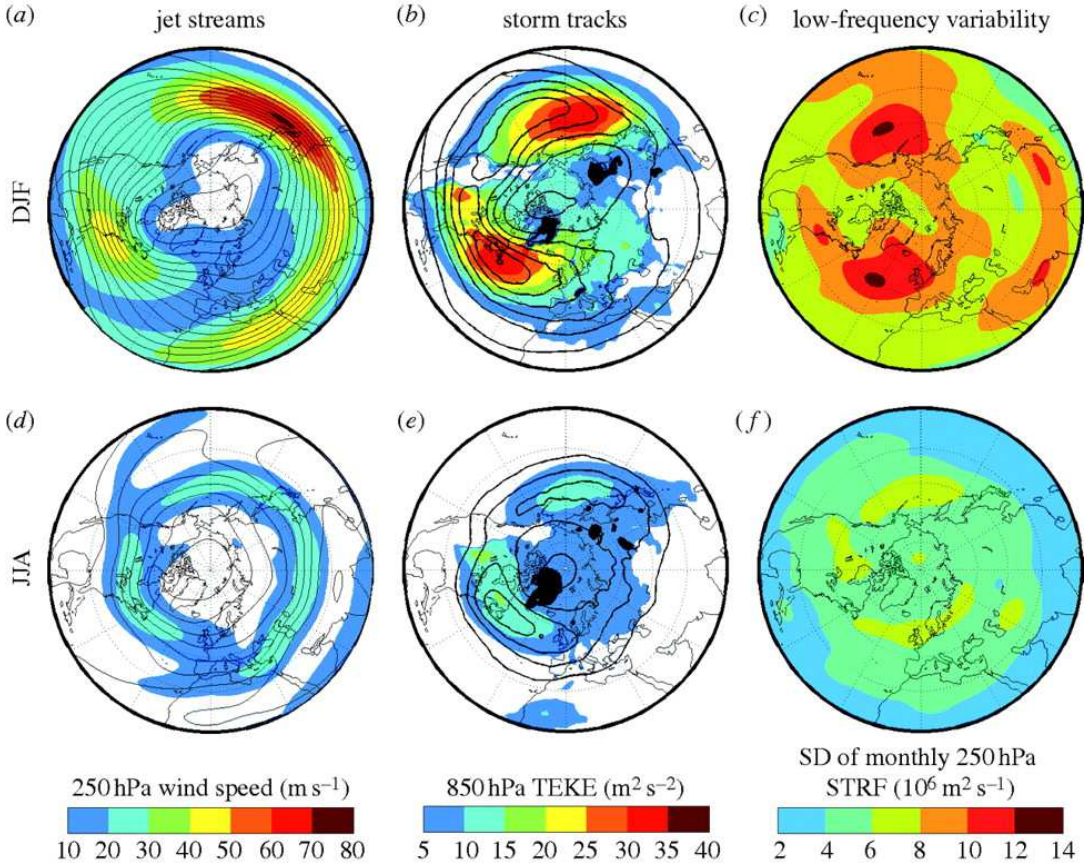

Figure 4.1. Northern Hemisphere climatology for December 1957 to August 2002 from the ERA-40 reanalysis (Uppala et al. 2005). (a) December–February (DJF) 250 hPa wind speed with streamfunction contoured every 1 × 10^7 m^2 s^−1. (b) DJF transient eddy kinetic energy (TEKE) using 2–6 day bandpass filtered winds. Shading shows low level values (850 hPa) and contour lines show the upper level (250 hPa) values contoured every 20m^2 s^−2. (c) Standard deviation of monthly-mean 250 hPa streamfunction in DJF. (d)–(f) are as (a)–(c) but for June–August (JJA). Figure from Woollings et al. 2010b.

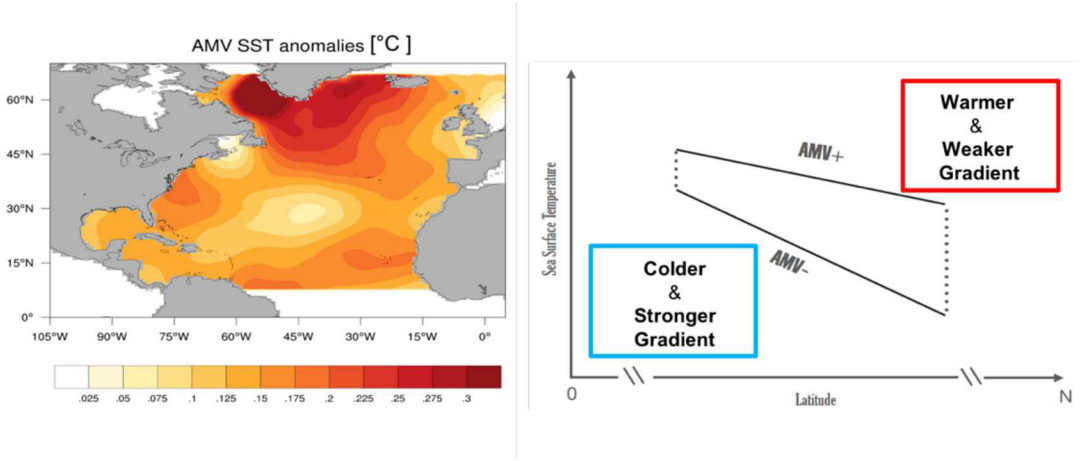

Figure 4.2. (left) Spatial pattern of the observed AMV SST anomalies (°C/σ_{AMV}) and (right) scheme of the state of the equator-to-pole temperature gradient in the AMV phases.

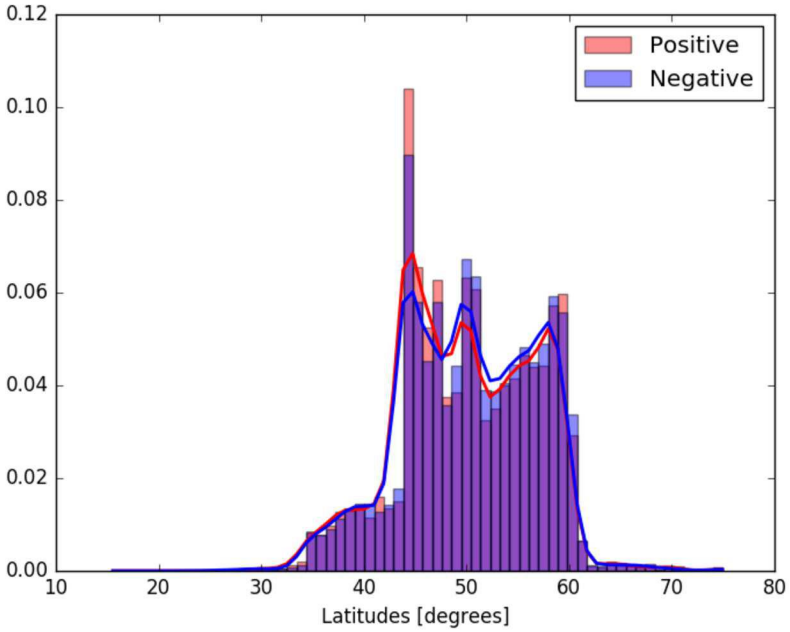

Figure 4.3. Probability Density Function (PDF) of the daily DJF jet stream latitude anomalies in AMV+(red) and AMV- (blue) experiments, averaged over 0°–60°W at 850 hPa. PDF is estimated following the Kernel method.

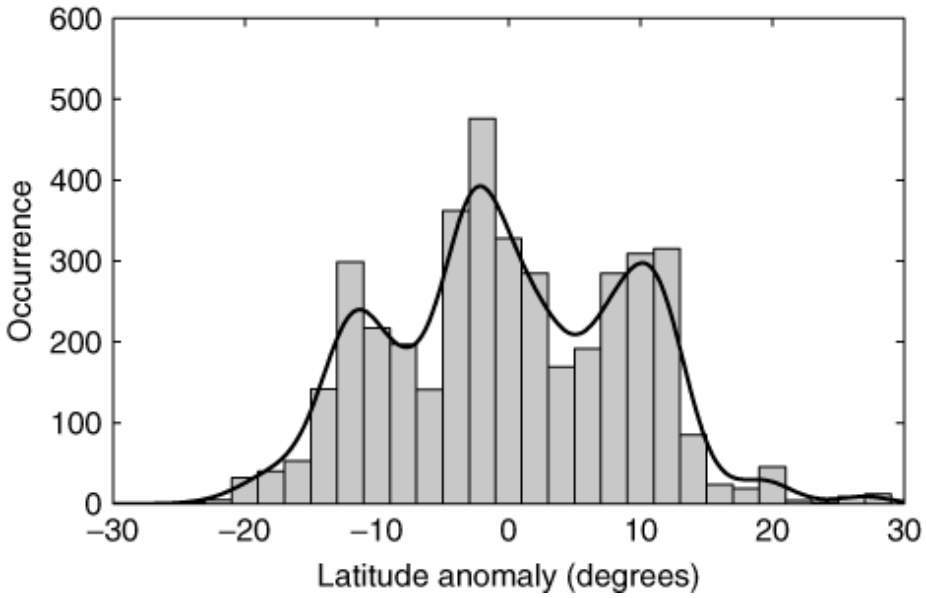

Figure 4.4. Probability Density Function (PDF) of the daily DJF jet stream latitude anomalies in ERA40 reanalysis, averaged over 0°–60°W and 925– 700 hPa. PDF is estimated following the Kernel method. Figure from Woollings et al. [2010a]

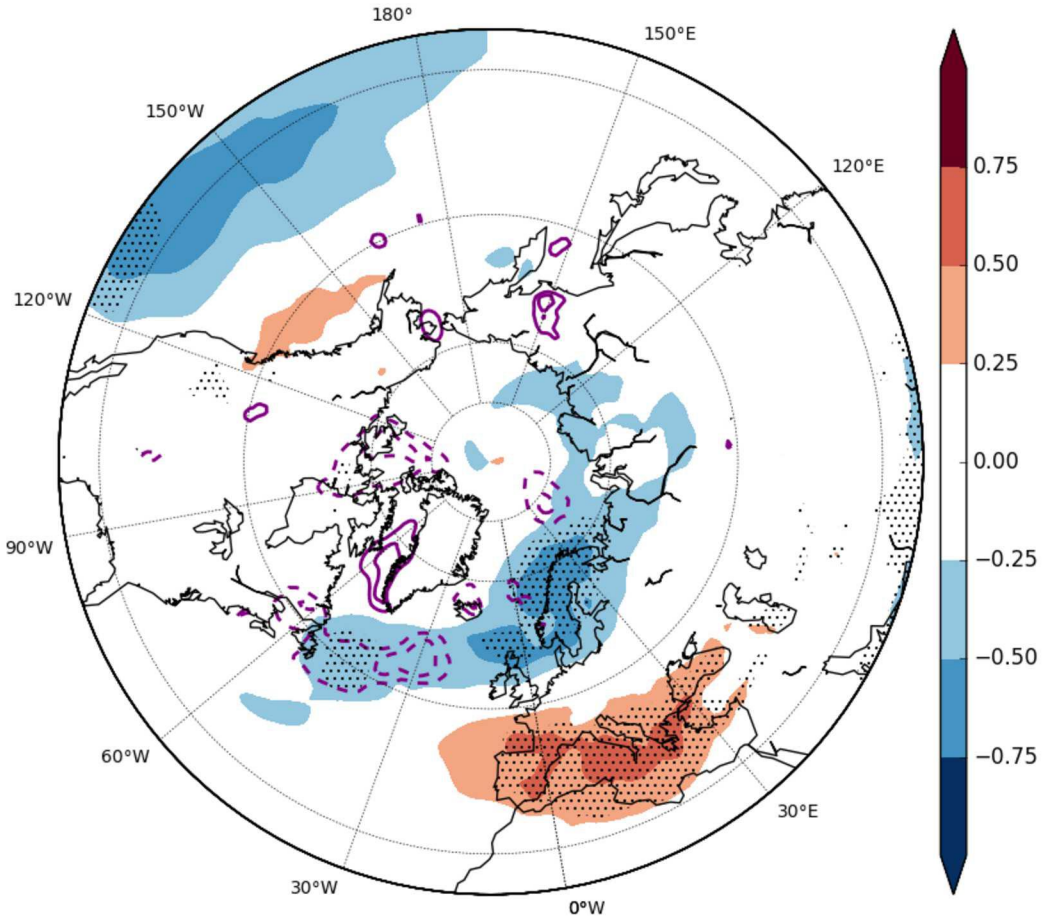

Figure 4.5. December-to-February season difference of the zonal wind at 850 hPa (U850, shaded areas, unit in m/s) and eddy heat transport at 850 hPa ($\overline{V'T'}$, contours interval at 0.5 K m/s). The statistical significance (stippling region) of U850 is evaluated by means of a two-tailed Student's t test, with a 95% confidence level, considering each year of the single ensemble member.

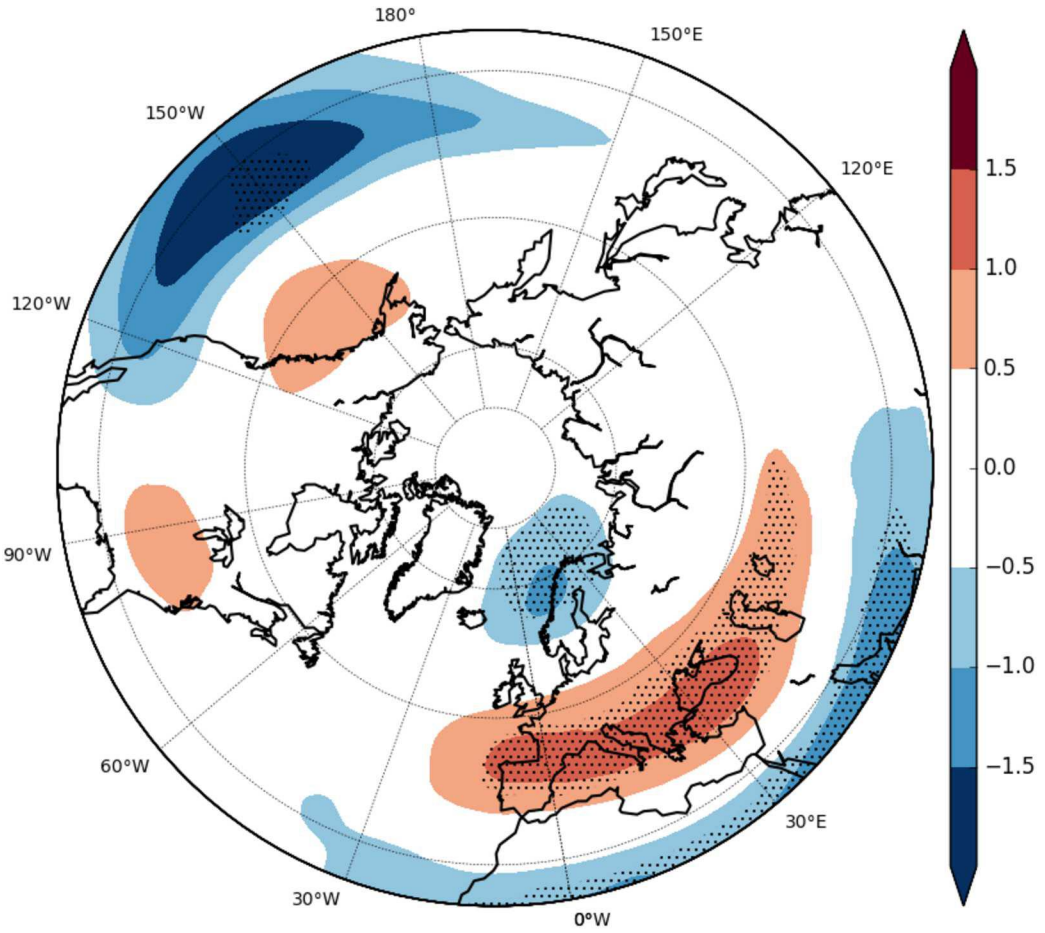

Figure 4.6. December-to-February season difference of the zonal wind at 200 hPa (U200), between the positive and negative phase of the AMV. Unit is m/s. The statistical significance (stippling region) is evaluated by means of a two-tailed Student's t test, with a 95% confidence level, considering each year of the single ensemble member.

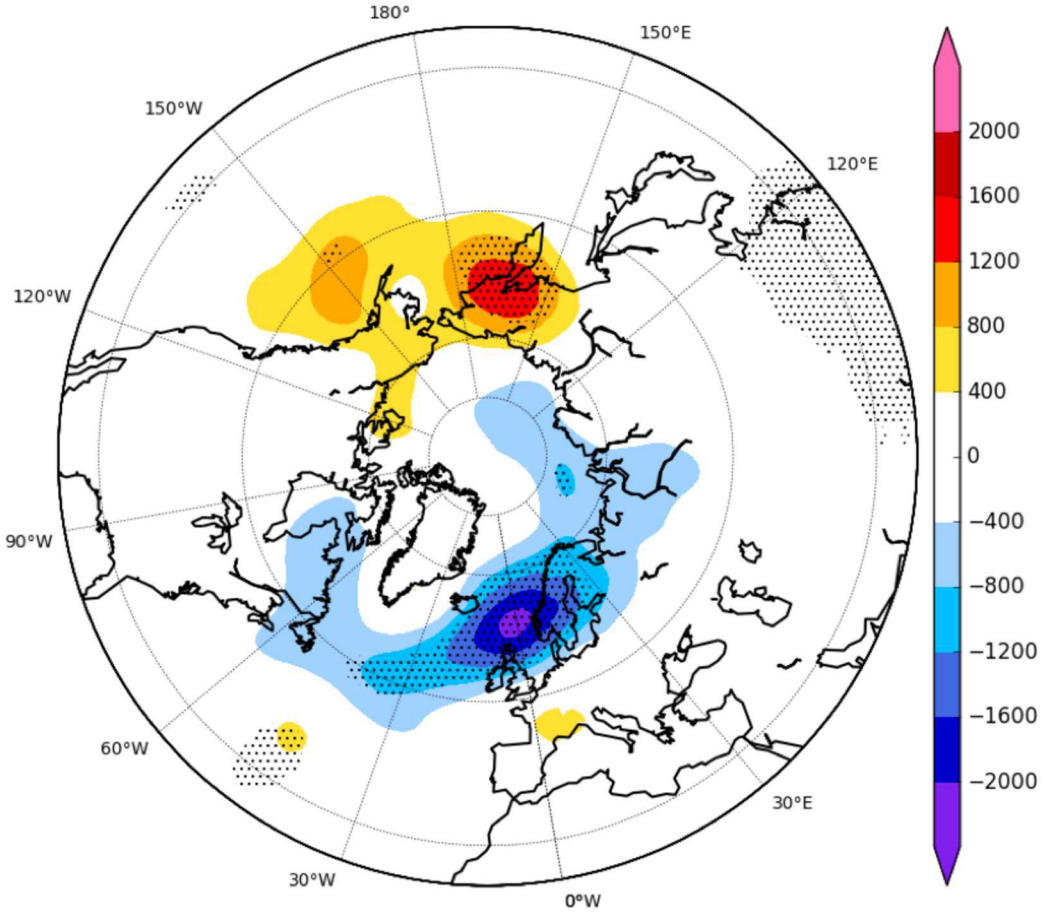

Figure 4.7. December-to-February season difference of the 9-day high-pass-filtered 500-hPa geopotential height variance between the positive and negative phase of the AMV. Unit is m². The statistical significance (stippling region) is evaluated by means of a two-tailed Student's t test, with a 95% confidence level, considering each year of the single ensemble member.

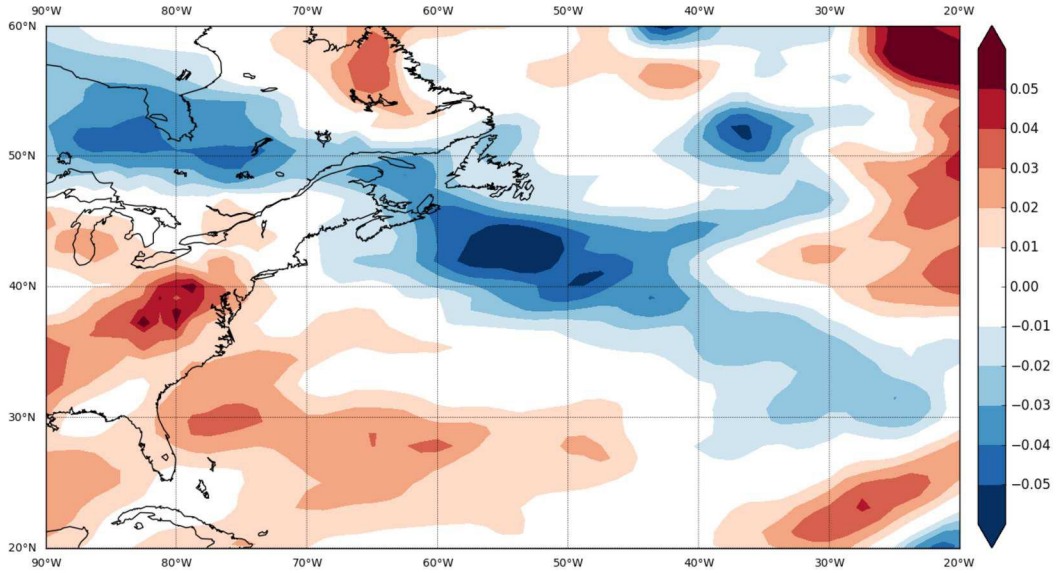

Figure 4.8. December-to-February season difference of the Eady Growth rate between the positive and negative phase of the AMV. Unit is d^{-1}. Available data only for 16 members.

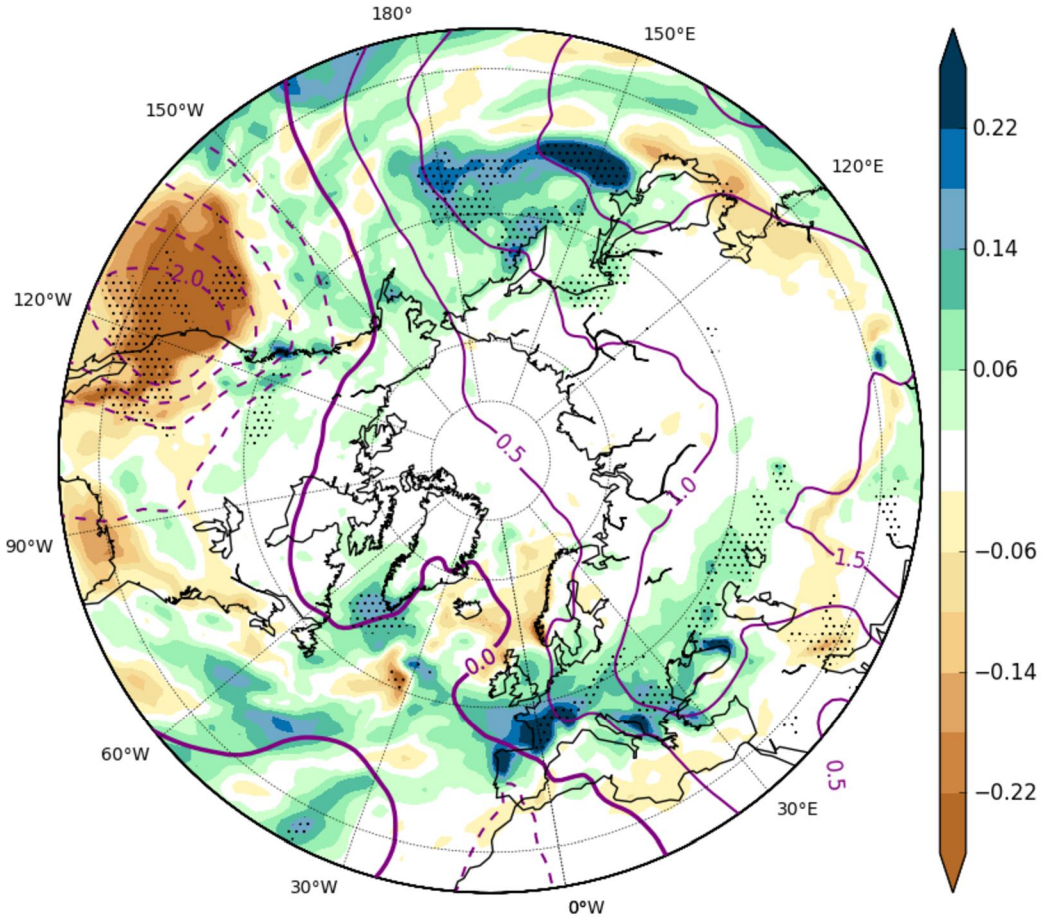

Figure 4.9. December-to-February season difference of precipitation (shaded areas, unit is mm/day) and Velocity Potential at 850 hPa (contours, unit is 0.1 x 10^6 m^2 s^{-1}). The statistical significance (stippling region) of precipitation is evaluated by means of a two-tailed Student's t test, with a 95% confidence level, considering each year of the single ensemble member. Note that colorbar changes compared to Figure 3.7 in order to highlight precipitation signal over Europe.

5 – *Multidecadal North Atlantic-Tropical Pacific teleconnection*

5.1 Introduction

The North Atlantic SST warming associated to the positive phase of the AMV has world-wide impact, not confined to the ocean basin and the neighboring continents. Recent works have emphasized the potential trans-basin linkage between the Atlantic and the Pacific oceans at low-frequency time scales. According to the existing literature [Kucharski et al. 2011, McGregor et al. 2014, Li et al. 2016, Kucharski et al. 2016a, Kucharski et al. 2016b, Zanchettin et al. 2016, Sun et al. 2017, Barcikowska et al. 2017], the AMV SST modifies the Walker circulation, reinforcing the trade winds over the Central-Eastern Pacific. This alters the thermocline and induces a La Niña-like pattern over the whole ocean. In this context, the AMV-experiment approach can help to investigate the Atlantic-Pacific teleconnection, providing a response which accounts for all climate components and their mutual interaction. Moreover, the nature of the performed idealized experiments provides some insights into the role of the North Atlantic natural variability in driving inter-basin anomalies, as well as, the climate impact over the Pacific due to the large-scale circulation changes.

5.2 Trans-basin linkage in AMV experiments

The simulated AMV phase increases the annual North Atlantic SST (Figure 5.1), mimicking a Gill-type response to an anti-symmetric heating [Gill 1980]. According to the Gill's solution, the heat source induces a below-average SLP and cyclonic low-

level wind anomalies, consistent with the AMV-induced SLP pattern (Figure 5.2). The 850-hPa velocity potential field (hereafter VP850) clearly shows dynamic convergence placed over the tropical West Atlantic in the Northern Hemisphere and the subsequent deep convection (Figure 5.3). Thus, the stemming rising flow diverges out in the upper level troposphere (200-hPa) driving anomalous subsidence over two different locations (Figure 5.4). Surprisingly, a weaker subsidence area is located off the Western U.S. coast while a more intense one is associated with the divergent wind which crosses the equator and converges in a stretched center between 10°S and 30°S. The descending flow reaches the lower atmosphere at ~130°W and a fraction of the 850-hPa divergent wind converges towards the Atlantic maximum, closing the trans-basin atmospheric cell (Figure 5.3). The remaining wind intensifies the trades winds which feeds the Indo-Pacific Walker circulation, enhancing the deep convection over the warm pool of the Maritime continent. A secondary, minor recirculation is also evident north the New Zealand. To better understand how the atmospheric circulation is modified along the Tropical belt, the equatorial Pacific cross section of the vertical velocity (ω), averaged between 5°S and 5°N, is presented. The ω field consistently shows the circulation anomalies along the Tropical Pacific, with upward (downward) motion represented by negative (positive) values (Figure 5.6). A strong subsidence in the Central Pacific and a deep convection increase at the boundaries of the basin underline the enhancement of the Walker circulation fostered by multidecadal variability of the North Atlantic SST.

An intriguing effect of the AMV-induced circulation is the response of the equatorial Pacific in terms of SST which closely resembles a La Niña-type pattern (Figure 5.1). Close to the Central America, westerly wind anomalies suppress the evaporation which prevents heat release from the ocean (Figure 5.2). Along the equatorial Pacific, easterly surface winds are reinforced through most of the basin and power the WES (Wind-Evaporation-SST) positive feedback, allowing heat transfer from

the ocean into the atmosphere. It is worth noting that a clear signature of this process is the emerging equatorial "cold tongue", the typical pattern of negative SST anomalies occurring during La-Niña condition along the equator. Furthermore, the western side of the basin shows above-average SST anomalies since the stronger trade winds prevent the eastward intrusion of warm water from the western equatorial Pacific. SST changes are consistent with the ocean subsurface temperature anomalies for an equatorial cross-section (Figure 5.7), revealing a cooling in the central and eastern side of the basin and a warming in the Western Pacific. The detected subsurface temperature zonal dipole suggests an upwelling of cold waters induced by the intensification of the easterlies. Over the Indian ocean, the trade winds are weakened by a westerly anomalous flow (Figure 5.2) which favors the establishment of positive temperature anomalies with a warm core at 100-m depth.

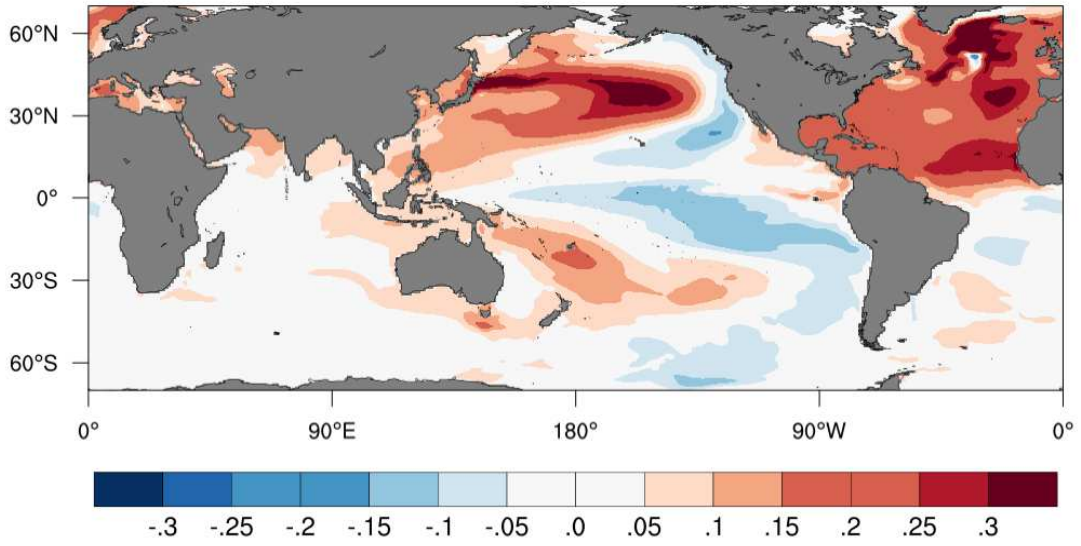

Figure 5.1. Differences between the last 8-year ensemble means of the positive and negative phases of the AMV experiments for sea surface temperature (unit is °C).

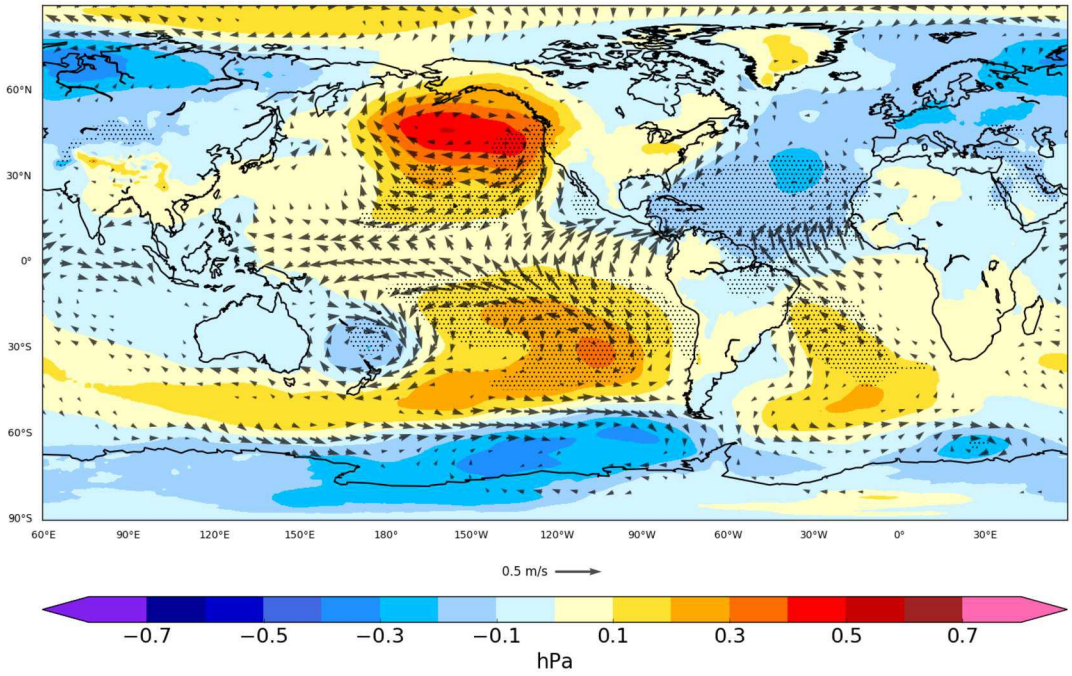

Figure 5.2. Differences between the last 8-year ensemble mean of the positive and negative phases of the AMV experiments for sea level pressure (shading, unit is hPa) and lowest-level wind (vectors, unit is m/s). Dotted regions display significant values for sea level pressure (Student's t test with 95% confidence level).

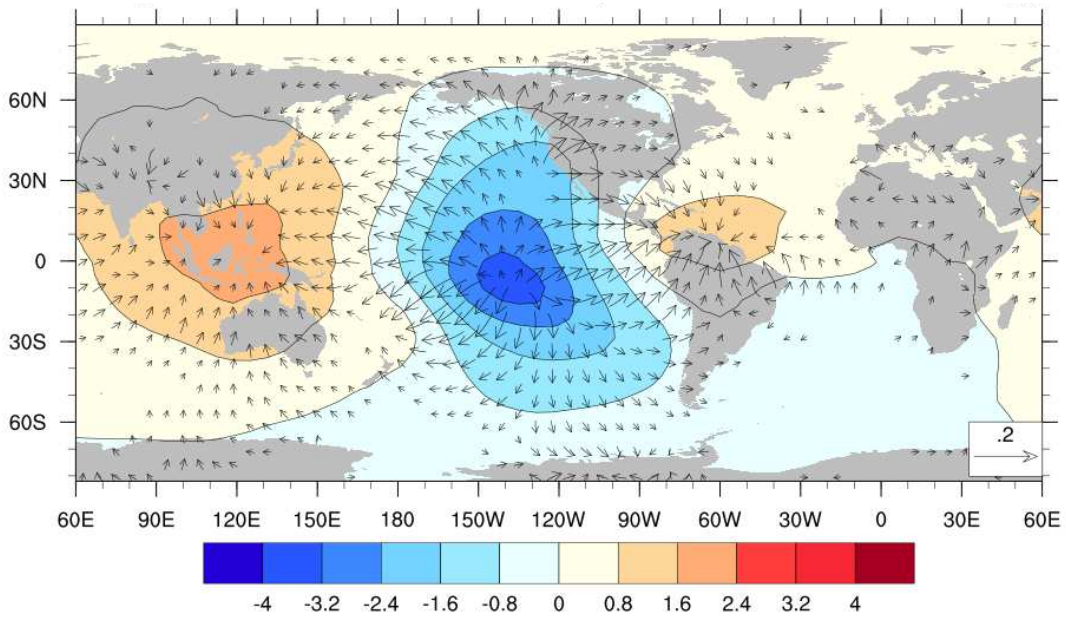

Figure 5.3. Same as Fig. 2 but for 850 hPa velocity potential (shaded colors, unit is 10^5 m^2 s^{-1}) and divergent wind (vectors, unit is m s^{-1}, omitted below 0.02 m s^{-1}).

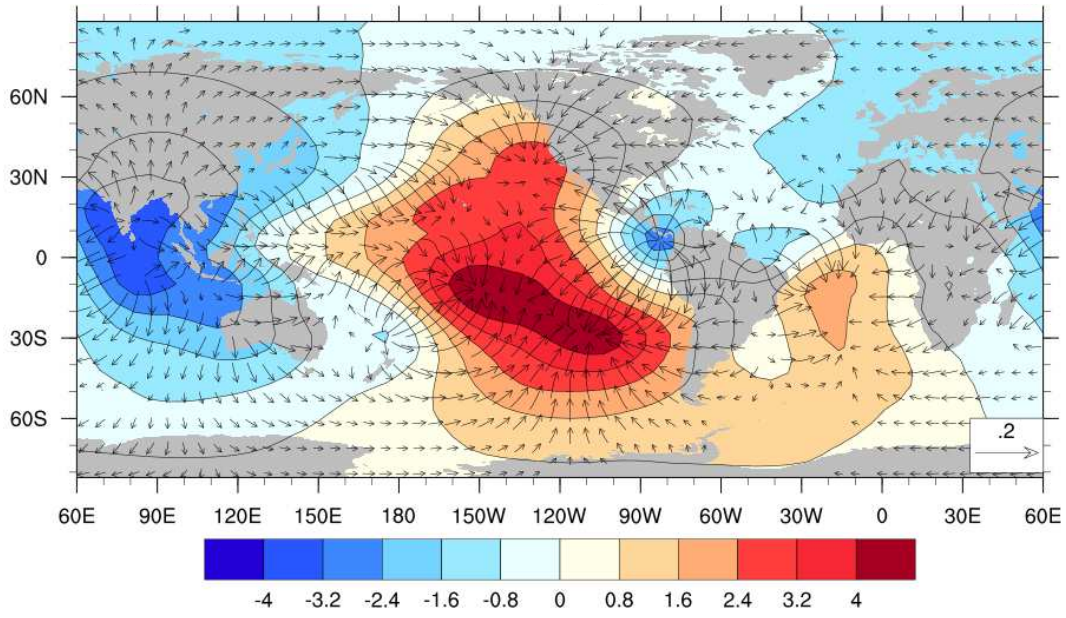

Figure 5.4 Same as Figure 5.3 but velocity potential at 200 hPa.

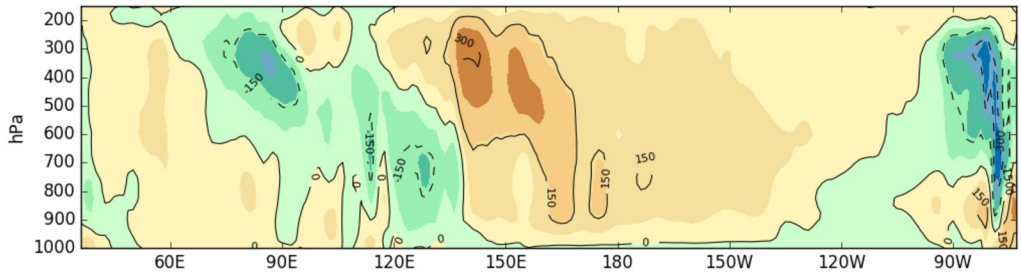

Figure 5.5. Differences between the last 8-year ensemble mean of the positive and negative phases of the AMV experiments for vertical velocity (ω, unit is 10^5 Pa s^{-1}) averaged between 5°S and 5°N.

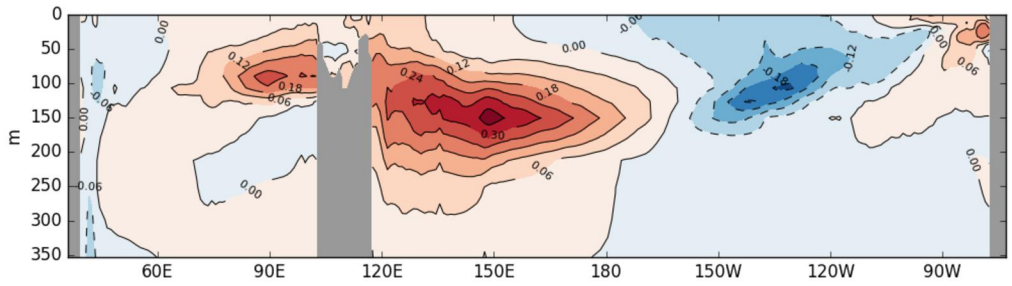

Figure 5.6. Differences between the last 8-year ensemble mean of the positive and negative phases of the AMV experiments for ocean temperature (unit is °C) averaged from 5°S and 5°N.

5.3 Summary and Discussions

In this chapter, the linkage between the AMV and the tropical Pacific is investigated. At multidecadal time scales, the AMV-associated atmospheric convection induces a modification of the Walker circulation with a tropical Pacific response which closely resembles a La Niña-like pattern.

The strong ascending motion over the North Atlantic during a positive phase of the AMV is consistent with the Gill's hypothesis [1980] about an extra-source of heating

placed north of the equator, as well as, with the Atlantic response in terms of negative SLP and cyclonic wind anomalies [Knight et al. 2006, Sutton and Hodson 2005, Sutton and Dong 2012]. The trans-basin linkage occurs at the high troposphere according to velocity potential field. In AMV experiments, most of the 200-hPa divergent wind converges south of the equator. This disagrees with Sun et al. study [2017] from which a zonal dipole of upper-level velocity potential emerges along the equator. One can speculate that, in AMV experiments, the anomalous divergence over Central America has shifted southwards the Eastern Pacific convergence, splitting the cell and generating a secondary, smaller amplitude convection region in the north-east Pacific. Interestingly, in another study, based on a very similar experimental protocol [Ruprich-Robert et al. 2018], it has found an analogous subsidence pattern over the California region, associated with an increase of heat waves occurrence during a warm phase of the AMV.

In the Pacific, the VP850 field clearly stresses the modification of the Walker cell, in line with previous studies [McGregor et al. 2014, Li et al. 2016, Kucharski et al. 2016a, Kucharski et al. 2016b, Ruprich-Robert et al. 2017, Sun et al. 2017, Barcikowska et al. 2017]. The model also successfully reproduces La Niña-like adjustment both in the ocean and in the atmosphere: on the tropical Eastern side, low-level westerly anomalies keep the heat in the subsurface ocean while the intensification of the trade winds over the Central Pacific enhances the WES feedback and induces the upwelling of cold water. In the Indian-Pacific side, enhanced deep convection reinforces the Walker circulation associated to lower SLP [Kucharski et al. 2015, Kucharski et al. 2016b].

The present results show the relevance of using a fully-coupled model, allowing ocean-atmosphere feedbacks to the imposed AMV anomalies, compared to analogous works based on atmosphere-only simulations. As an example, the lack of ocean-atmosphere coupled interactions generates a completely different pattern from the

detected La Niña-like response, as in the case of a stand-alone atmospheric model with prescribed SSTs [Li et al. 2016].

From a broader perspective, the teleconnection of the AMV to the Tropical Pacific is of primary importance in light of multidecadal climate change. A prominent cooling of the Eastern Pacific is occurring during the last 20 years compared to the 1970-2000 period [Kosaka and Xie 2013, Meehl and Teng 2014, McGregor et al. 2014]. Trade winds reinforcement and a negative La Niña-type signature in the Pacific have been linked to the Atlantic warming trend of the last decades associated to a negative NAO arisen at the beginning of the 90s [Kucharski et al. 2011, Yeager et al. 2012, Chikamoto et al. 2012, Robson et al. 2012, Chikamoto et al. 2015]. The present AMV experiments are able to not only reproduce the Pacific symptoms recorded during the 90's, but it assesses the climate impact thereto. In addition, keeping the simulated external forcings at the pre-industrial values highlights the role of the North Atlantic internal variability in modulating trans-basin climate connections at decadal or longer time scales [Kucharski et al. 2016b].

Summary and Conclusions

Aims of this study are to numerically represent and analyze the climate response to internal and low-frequency Sea Surface Temperature (SST) variability imposed in the North Atlantic Ocean. We intended to address how the Atlantic SST can modulate ocean temperature variability and drives global and regional climate. This thesis contributes to a better understanding of the mechanisms associated with these SST fluctuations, referred to as the Atlantic Multidecadal Variability (AMV). In particular, the thesis addresses a range of scientific issues involving the global and dynamical response to AMV anomalies, including the explanation of physical mechanisms such as the meridional shift of the eddy-driven jet and the teleconnection between the North Atlantic and the Tropical Pacific.

The world-wide response to the AMV anomalies is assessed to provide a global view of how such multidecadal SST fluctuations can impact the climate system, even far from the source of variability. Global impact has been evaluated as the difference between the positive and negative phase of the AMV both in boreal summer and winter, to highlight the seasonal dependent response of the climate system under a year-round perturbation.

For this purpose, a suite of experiments has been performed with the CMCC-CM2-SR5 coupled climate model, following the experimental protocol for the component C of the Decadal Climate Prediction Project (DCPP) contribution to CMIP6 (detailed in Boer et al. 2016). In these idealized experiments, the methodological approach requires that the model North Atlantic SST is periodically restored towards an estimate of the internal component of the observed AMV, while the model can freely evolve outside the restored region, allowing full climate system response. Positive (negative) time-independent anomaly is considered to simulate the warm (cold) AMV phase. The

differences between the simulated positive and negative phases are analyzed in order to capture the linear climate response to the AMV.

Furthermore, to validate the model results, a comparison with a second set of simulations is proposed, computed by the CNRM-CM5 coupled model (based on the same experimental protocol) and made available by the GLOBC group from CERFACS.

The climate impacts reproduced in numerical calculations stress the role of the AMV in driving marked changes in terms of air temperature, precipitation and synoptic circulation at global scale. As expected, greater anomalies are found over the Northern Hemisphere, characterized by strong seasonal signals. Boreal summer (from June to September) shows an unequivocal northward shift and a strengthening of the upper part of the Inter-Tropical Convergence Zone (ITCZ) leading to increased rainfall over the Atlantic equatorial belt, including the semiarid Sahel region and Central America. North-East Brazil directly experiences the seasonal ITCZ shift with dry summer and wet winter anomalies during a positive AMV. These precipitation anomalies alter the large-scale circulation, promoting an upward motion over the tropical Atlantic. Moreover, Eastern Europe exhibits an anomalous warming in agreement with the increasing trend observed during the last decades, fostering the link between AMV and the extreme dry periods in that region [e.g. Cassou et al. 2005]. The multidecadal variation of the North Atlantic SST also affects remote areas of the globe such as the Indian region where above-normal convective precipitation is found during the summer monsoon rainfall season.

During boreal Winter (from December to March), significant warming covers the Southern Eurasia and Arctic Ocean in both the models (~0.6°C). The latter may seriously undermine the Arctic sea-ice cover at the end of the melting season, leading to an anomalous decline of the albedo and, potentially, exciting a positive feedback. Along the equatorial belt, precipitation is intensified by the northward shift of the

winter ITCZ, extending rainfall over the Tropical South America. The AMV projects the Pacific Ocean onto the negative phase of the Interdecadal Pacific Oscillation (IPO), characterized by a zonal gradient of 2-m temperature anomalies. Unlike the CMCC results and literature background, CNRM model shows positive zonal anomalies which cover the tropical Pacific, breaking the negative IPO pattern. Nevertheless, marked weakening of the Aleutian low occurs in the North Pacific in both the models, associated to a drop in the mean, cyclonic advection, cooling the North-Western America.

Despite the seasonal responses, some climate impact persists throughout the year suggesting a direct link to the imposed warming over the Atlantic. For instance, a subsidence zone is found over South-West U.S., characterized by above-average air temperature at surface along with reduced precipitation which may lead to an increase of heat-wave events in that region [Ruprich-Robert et al. 2018]. The West Tropical Pacific (WTP) represents another peculiar zone where the AMV-associated anomalies keeping their sign and module all year long. Significant increase of convective precipitation and 2-m temperature suggest a mechanism that, induced by the multidecadal North Atlantic SST variability, is continuously fed by large-scale circulation anomalies.

A modified Signal-to-Noise Ratio analysis is used to quantify the predictive skill of the AMV impact. This metrics allows to estimate the proportion of the decadal variance forced by the AMV. Surprisingly, in the hypothesis of successfully predicting the AMV phase, a SNR analysis reveals high predictive skill of the summer warming over the Mediterranean region and North-West America (~30%), and even stronger over South-West U.S. and North-East Brazil (more than 45%). During Boreal winter, weak SNR is noticeable over land. Nevertheless, the AMV accounts for, at least, the 40% of the ITCZ-shift variance throughout the year between the two models. The persistence of this feature is intriguing because it may be one of the potential signatures of the

AMV. The WTP warming is also partially predictable both in summer and winter (up to 25%), in line with the teleconnection found between the North Atlantic and the Tropical Pacific.

Discrepancies over the European region between the two models and the weak SNR during wintertime have highlighted the need to further investigate on the effect of the AMV on the large-scale atmospheric circulation over the North Atlantic. The behavior of the eddy-driven jet stream under AMV-induced variability is analyzed in CMCC model results. The imposed pattern of SST decreases the meridional temperature gradient in the North Atlantic, especially during wintertime, since the AMV-related largest anomalies straddle an area characterized by a strong baroclinicity. During a positive AMV phase, a consistent reduction of the eddy heat transport of about 0.5 – 1.0 K m s^{-1} occurs over the ocean region off the Canadian seaboard, leading to a southward shift of the North Atlantic Jet (NAJ) of ~6° latitude and corroborating the hypothesis that the AMV modulates the meridional position of the eddy-driven jet stream. This result clarifies some aspects of the European climate, such as the AMV-induced increased rainfall associated to an extra transport of moist air along the modified NAJ path.

Interestingly, the Tropical Pacific shows significant AMV-induced features, such as a negative Interdecadal Pacific Oscillation signature in the air temperature field, which persist throughout the year. This is in line with the existing literature arguing that the multidecadal variability of the North Atlantic SST modulates excites the Pacific Ocean via atmospheric bridge. The investigated mechanism in CMCC model highlights how the Walker circulation is modified by the inter-hemispheric energy imbalance due to the positive AMV polarity. From warm North Atlantic Ocean, an ascending flow reaches the upper troposphere and mostly sinks in the equatorial Pacific, linking the two basins. Anomalous surface winds zonally diverge from the subsidence

area along the equatorial Pacific. On the East, the anomalous westerlies weaken the trade winds suppressing the Wind-Evaporation-SST (WES) feedback and preventing heat release from the ocean into the atmosphere. On the contrary, in the Western-Central Pacific, enhanced easterly winds steps up the WES feedback, decreasing the local SST, and prevents the eastward breach of surface warm waters from the Indo-Western Pacific. Anomalies of atmospheric vertical velocity clearly shows this double-cell circulation, with upward flows over the Indonesia and Mexico and a downward flow in the Central Pacific (~130°W), inducing a La Niña-like in response to the anomalous low-level winds. Furthermore, the intensified trade winds alter the thermocline over the equatorial Pacific, with the development of warm and cold cores in the oceanic subsurface and the resulting upwelling of cool waters, in agreement with Li et al. work [2016]. Surprisingly, these findings partially explain the "hiatus" occurred from the early 2000s, which has contributed to the global temperature drop, as a lagged equatorial Pacific response to a cold-to-warm AMV phase transition. The linkage may also enlighten about the potential role of the AMV as source of predictability.

Overall, this study points out the world-wide impact of the multidecadal variability of the North Atlantic SST, emphasizing the evident and relevant role that AMV plays in modulating recent and future climate change and multidecadal variability.

List of Abbreviations

AMO	Atlantic Multidecadal Oscillation
AMOC	Atlantic Meridional Overturning Circulation
AMV	Atlantic Multidecadal Variability
CAM	Community Atmospheric Model
CERFACS	Centre Européen de Recherche et de Formation Avancée en Calcul Scientifique
CESM	Community Earth System Model
CMCC	Euro-Mediterranean Centre on Climate Change
CMIP	Coupled Model Intercomparison Project
CML	Community Land Model
CNRM	Centre National de Recherches Météorologiques
C_P	Constant pressure specific heat
DCPP	Decadal Climate Predictions Project
DJFM	December-to-March
EAP	East Atlantic Pattern
ENSO	El Niño–Southern Oscillation
EOF	Empirical Orthogonal Function
ERSSTv4	Extended Reconstructed Sea Surface Temperature version 4
GHG	Greenhouse Gases
hfcorr	Heat flux restoring term
IPO	Interdecadal Pacific Oscillation
ISM	Indian Summer Monsoon
ITCZ	Inter-Tropical Convergence Zone

JJAS	June-to-September
MLD	Mixed Layer Depth
NAE	North Atlantic and European
NAJ	North Atlantic Jet
NAO	North Atlantic Oscillation
NCEP-NCAR	National Centers for Environmental Prediction – National Center for Atmospheric Research
NEMO	Nucleus for European Modelling of the Ocean
PC1	first Principal Component
PDF	Probability Density Function
PDO	Pacific Decadal Oscillation
PNA	Pacific-North America
RCP8.5	Representation Concentration Pathway 8.5
RR_T	Temperature Restoring Rate
SAT	Surface Air Temperature
SLP	Sea-Level Pressure
SNP	Subtropical North Pacific
SNR	Signal-to-total-variance ratio
SPCZ	South Pacific Convergence Zone
SPG	Subpolar Gyre
SST	Sea Surface Temperature
WES	Wind-Evaporation-SST
WTP	Western Tropical Pacific

Bibliography

Arguez, A., O'Brien, J. J., & Smith, S. R. (2009). Air temperature impacts over Eastern North America and Europe associated with low-frequency North Atlantic SST variability. International Journal of Climatology: A Journal of the Royal Meteorological Society, 29(1), 1-10.

Athanasiadis, P. J., Wallace, J. M., & Wettstein, J. J. (2010). Patterns of wintertime jet stream variability and their relation to the storm tracks. Journal of the Atmospheric Sciences, 67(5), 1361-1381.

Ba, J., Keenlyside, N. S., Latif, M., Park, W., Ding, H., Lohmann, K., ... & y Melia, D. S. (2014). A multi-model comparison of Atlantic multidecadal variability. *Climate dynamics*, 43(9-10), 2333-2348.

Barcikowska, M. J., Knutson, T. R., & Zhang, R. (2017). Observed and simulated fingerprints of multidecadal climate variability and their contributions to periods of global SST stagnation. Journal of Climate, 30(2), 721-737.

Barnston, A. G., & Livezey, R. E. (1987). Classification, seasonality and persistence of low-frequency atmospheric circulation patterns. Monthly weather review, 115(6), 1083-1126.

Barton, N. P., & Ellis, A. W. (2009). Variability in wintertime position and strength of the North Pacific jet stream as represented by re-analysis data. International Journal of Climatology, 29(6), 851-862.

Bellucci, A., Mariotti, A., & Gualdi, S. (2017). The role of forcings in the twentieth-century North Atlantic multidecadal variability: The 1940–75 North Atlantic cooling case study. Journal of Climate, 30(18), 7317-7337.

Beszczynska-Möller, A., Woodgate, R. A., Lee, C., Melling, H., & Karcher, M. (2011). A synthesis of exchanges through the main oceanic gateways to the Arctic Ocean. Oceanography, 24(3), 82-99.

Bjerknes, J. (1964). Atlantic air-sea interaction. *Advances in geophysics*, 10, 1-82.

Bjerknes, J. (1969). Atmospheric teleconnections from the equatorial Pacific. Monthly weather review, 97(3), 163-172.

Blackmon, M. L. (1976). A climatological spectral study of the 500 mb geopotential height of the Northern Hemisphere. Journal of the Atmospheric Sciences, 33(8), 1607-1623.

Boer, G. J., Smith, D. M., Cassou, C., Doblas-Reyes, F., Danabasoglu, G., Kirtman, B., ... & Mueller, W. A. (2016). The Decadal Climate Prediction Project, *Geosci. Model Dev. Discuss.*, doi: 10.5194.

Booth, B. B., Dunstone, N. J., Halloran, P. R., Andrews, T., & Bellouin, N. (2012). Aerosols implicated as a prime driver of twentieth-century North Atlantic climate variability. Nature, 484(7393), 228.

Branstetter, M. L., & Famiglietti, J. S. (1999). Testing the sensitivity of GCM-simulated runoff to climate model resolution using a parallel river transport algorithm. In Preprints, 14th Conf. on Hydrology, Dallas, TX, Amer. Meteor. Soc (pp. 391-392).

Brönnimann, S. (2007). Impact of El Niño–southern oscillation on European climate. Reviews of Geophysics, 45(3).

Cassou, C., Deser, C., Terray, L., Hurrell, J. W., & Drévillon, M. (2004). Summer sea surface temperature conditions in the North Atlantic and their impact upon the atmospheric circulation in early winter. Journal of Climate, 17(17), 3349-3363.

Cassou, C., Terray, L., & Phillips, A. S. (2005). Tropical Atlantic influence on European heat waves. Journal of climate, 18(15), 2805-2811.

Cassou, C. (2008). Intraseasonal interaction between the Madden–Julian oscillation and the North Atlantic Oscillation. Nature, 455(7212), 523.

Cherchi, A., Fogli, P.G., Lovato, T., Peano, D., Iovino, D., Gualdi, S., Masina, S., Scoccimarro, E., Materia, S., Bellucci, A., & Navarra, A. (in review). Journal of Advances in Modeling Earth Systems.

Chikamoto, Y., Mochizuki, T., Timmermann, A., Kimoto, M., & Watanabe, M. (2016). Potential tropical Atlantic impacts on Pacific decadal climate trends. *Geophysical Research Letters*, 43(13), 7143-7151.

Chylek, P., Folland, C. K., Lesins, G., Dubey, M. K., & Wang, M. (2009). Arctic air temperature change amplification and the Atlantic Multidecadal Oscillation. Geophysical Research Letters, 36(14).

Chylek, P., Folland, C., Frankcombe, L., Dijkstra, H., Lesins, G., & Dubey, M. (2012). Greenland ice core evidence for spatial and temporal variability of the Atlantic Multidecadal Oscillation. Geophysical Research Letters, 39(9).

Davidson, E. A., de Araújo, A. C., Artaxo, P., Balch, J. K., Brown, I. F., Bustamante, M. M., ... & Munger, J. W. (2012). The Amazon basin in transition. Nature, 481(7381), 321.

Davini, P., von Hardenberg, J., & Corti, S. (2015). Tropical origin for the impacts of the Atlantic Multidecadal Variability on the Euro-Atlantic climate. Environmental Research Letters, 10(9), 094010.

Day, J. J., Hargreaves, J. C., Annan, J. D., & Abe-Ouchi, A. (2012). Sources of multi-decadal variability in Arctic sea ice extent. *Environmental Research Letters*, 7(3), 034011.

Dee, D. P., Uppala, S. M., Simmons, A. J., Berrisford, P., Poli, P., Kobayashi, S., ... & Bechtold, P. (2011). The ERA-Interim reanalysis: Configuration and performance of the data assimilation system. Quarterly Journal of the royal meteorological society, 137(656), 553-597.

Delworth, T. L., & Knutson, T. R. (2000). Simulation of early 20th century global warming. Science, 287(5461), 2246-2250.

Delworth, T. L., Broccoli, A. J., Rosati, A., Stouffer, R. J., Balaji, V., Beesley, J. A., ... & Durachta, J. W. (2006). GFDL's CM2 global coupled climate models. Part I: Formulation and simulation characteristics. Journal of Climate, 19(5), 643-674.

Delworth, T. L., Zeng, F., Zhang, L., Zhang, R., Vecchi, G. A., & Yang, X. (2017). The central role of ocean dynamics in connecting the North Atlantic Oscillation to the extratropical component of the Atlantic Multidecadal Oscillation. Journal of Climate, 30(10), 3789-3805.

Deser, C., & Timlin, M. S. (1997). Atmosphere–ocean interaction on weekly timescales in the North Atlantic and Pacific. Journal of climate, 10(3), 393-408.

Donohoe, A., Marshall, J., Ferreira, D., Armour, K., & McGee, D. (2014). The interannual variability of tropical precipitation and interhemispheric energy transport. Journal of Climate, 27(9), 3377-3392.

Drinkwater, K. F., Miles, M., Medhaug, I., Otterå, O. H., Kristiansen, T., Sundby, S., & Gao, Y. (2014). The Atlantic Multidecadal Oscillation: Its manifestations and impacts with special emphasis on the Atlantic region north of 60 N. Journal of Marine Systems, 133, 117-130.

Edwards, M., Beaugrand, G., Helaouët, P., Alheit, J., & Coombs, S. (2013). Marine ecosystem response to the Atlantic Multidecadal Oscillation. PLoS One, 8(2), e57212.

Eichelberger, S. J., & Hartmann, D. L. (2007). Zonal jet structure and the leading mode of variability. Journal of Climate, 20(20), 5149-5163.

Eldevik, T., Nilsen, J. E. Ø., Iovino, D., Olsson, K. A., Sandø, A. B., & Drange, H. (2009). Observed sources and variability of Nordic seas overflow. Nature Geoscience, 2(6), 406.

Enfield, D. B., Mestas-Nuñez, A. M., & Trimble, P. J. (2001). The Atlantic multidecadal oscillation and its relation to rainfall and river flows in the continental US. Geophysical Research Letters, 28(10), 2077-2080.

Farneti, R. (2017). Modelling interdecadal climate variability and the role of the ocean. *Wiley Interdisciplinary Reviews: Climate Change*, 8(1).

Fogli, P. G., & Iovino, D. (2014). CMCC–CESM–NEMO: Toward the New CMCC Earth System Model.

Folland, C. K., Palmer, T. N., & Parker, D. E. (1986). Sahel rainfall and worldwide sea temperatures, 1901–85. Nature, 320(6063), 602.

Frankcombe, L. M., Von Der Heydt, A., & Dijkstra, H. A. (2010). North Atlantic multidecadal climate variability: an investigation of dominant time scales and processes. Journal of climate, 23(13), 3626-3638.

Franzke, C., Lee, S., & Feldstein, S. B. (2004). Is the North Atlantic Oscillation a breaking wave?. Journal of the atmospheric sciences, 61(2), 145-160.

García-Serrano, J., & Doblas-Reyes, F. J. (2012). On the assessment of near-surface global temperature and North Atlantic multi-decadal variability in the ENSEMBLES decadal hindcast. Climate dynamics, 39(7-8), 2025-2040.

Gastineau, G., & Frankignoul, C. (2012). Cold-season atmospheric response to the natural variability of the Atlantic meridional overturning circulation. *Climate dynamics*, 39(1-2), 37-57.

Gastineau, G., & Frankignoul, C. (2015). Influence of the North Atlantic SST variability on the atmospheric circulation during the twentieth century. *Journal of Climate*, 28(4), 1396-1416.

Gerber, E. P., & Vallis, G. K. (2009). On the zonal structure of the North Atlantic Oscillation and annular modes. Journal of the Atmospheric Sciences, 66(2), 332-352.

Gill, A. (1980). Some simple solutions for heat-induced tropical circulation. Quarterly Journal of the Royal Meteorological Society, 106(449), 447-462.

Goldenberg, S. B., Landsea, C. W., Mestas-Nuñez, A. M., & Gray, W. M. (2001). The recent increase in Atlantic hurricane activity: Causes and implications. Science, 293(5529), 474-479.

Goswami, B. N., Venugopal, V., Sengupta, D., Madhusoodanan, M. S., & Xavier, P. K. (2006). Increasing trend of extreme rain events over India in a warming environment. Science, 314(5804), 1442-1445.

Gray, S. T., Graumlich, L. J., Betancourt, J. L., & Pederson, G. T. (2004). A tree-ring based reconstruction of the Atlantic Multidecadal Oscillation since 1567 AD. Geophysical Research Letters, 31(12).

Green, B., Marshall, J., & Donohoe, A. (2017). Twentieth century correlations between extratropical SST variability and ITCZ shifts. Geophysical Research Letters, 44(17), 9039-9047.

Häkkinen, S., Rhines, P. B., & Worthen, D. L. (2011). Atmospheric blocking and Atlantic multidecadal ocean variability. Science, 334(6056), 655-659.

Hannachi, A., Woollings, T., & Fraedrich, K. (2012). The North Atlantic jet stream: A look at preferred positions, paths and transitions. Quarterly Journal of the Royal Meteorological Society, 138(665), 862-877.

Hawkins, E., Smith, R. S., Gregory, J. M., & Stainforth, D. A. (2016). Irreducible uncertainty in near-term climate projections. *Climate Dynamics, 46*(11-12), 3807-3819.

Hoskins, B. J., James, I. N., & White, G. H. (1983). The shape, propagation and mean-flow interaction of large-scale weather systems. Journal of the atmospheric sciences, 40(7), 1595-1612.

Huang, B., Banzon, V. F., Freeman, E., Lawrimore, J., Liu, W., Peterson, T. C., ... & Zhang, H. M. (2015). Extended reconstructed sea surface temperature version 4 (ERSST. v4). Part I: upgrades and intercomparisons. Journal of climate, 28(3), 911-930.

Hunke, E. C., & Lipscomb, W. H. (2008). CICE: The Los Alamos sea ice model user's manual, version 4. Los Alamos National Laboratory Tech. Rep. LA-CC-06-012.

Hurrell, J. W. (1995). Decadal trends in the North Atlantic Oscillation: regional temperatures and precipitation. Science, 269(5224), 676-679.

Hurrell, J. W., & Folland, C. K. (2002). A change in the summer atmospheric circulation over the North Atlantic. Clivar Exchanges, 25(7), 52-54.

Hurrell, J. W., Kushnir, Y., Ottersen, G., & Visbeck, M. (2003). An overview of the North Atlantic oscillation. The North Atlantic Oscillation: climatic significance and environmental impact, 134, 1-35.

Hurrell, J. W., & Deser, C. (2010). North Atlantic climate variability: the role of the North Atlantic Oscillation. Journal of Marine Systems, 79(3-4), 231-244.

Joshi, M. K., & Rai, A. (2015). Combined interplay of the Atlantic multidecadal oscillation and the interdecadal Pacific oscillation on rainfall and its extremes over Indian subcontinent. Climate Dynamics, 44(11-12), 3339-3359.

Joshi, M. K., & Ha, K. J. (2018). Fidelity of CMIP5-simulated teleconnection between Atlantic multidecadal oscillation and Indian summer monsoon rainfall. Climate Dynamics, 1-20.

Kay, J. E., Deser, C., Phillips, A., Mai, A., Hannay, C., Strand, G., ... & Holland, M. (2015). The Community Earth System Model (CESM) large ensemble project: A community resource for studying climate change in the presence of internal climate variability. Bulletin of the American Meteorological Society, 96(8), 1333-1349.

Kerr, R. A. (2000). A North Atlantic climate pacemaker for the centuries. Science, 288(5473), 1984-1985.

Kinnard, C., Zdanowicz, C. M., Fisher, D. A., Isaksson, E., de Vernal, A., & Thompson, L. G. (2011). Reconstructed changes in Arctic sea ice over the past 1,450 years. Nature, 479(7374), 509.

Kirtman, B., Power, S. B., Adedoyin, A. J., Boer, G. J., Bojariu, R., Camilloni, I., ... & Prather, M. (2013). Near-term climate change: projections and predictability.

Knight, J. R., Allan, R. J., Folland, C. K., Vellinga, M., & Mann, M. E. (2005). A signature of persistent natural thermohaline circulation cycles in observed climate. Geophysical Research Letters, 32(20).

Knight, J. R., Folland, C. K., & Scaife, A. A. (2006). Climate impacts of the Atlantic multidecadal oscillation. *Geophysical Research Letters*, 33(17).

Knudsen, M. F., Seidenkrantz, M. S., Jacobsen, B. H., & Kuijpers, A. (2011). Tracking the Atlantic Multidecadal Oscillation through the last 8,000 years. Nature communications, 2, 178.

Komatsu, K. K., Alexeev, V. A., Repina, I. A., & Tachibana, Y. (2018). Poleward upgliding Siberian atmospheric rivers over sea ice heat up Arctic upper air. Scientific reports, 8(1), 2872.

Kosaka, Y., & Xie, S. P. (2013). Recent global-warming hiatus tied to equatorial Pacific surface cooling. *Nature*, 501(7467), 403-407.

Krishnamurthy, L., & Krishnamurthy, V. (2016). Teleconnections of Indian monsoon rainfall with AMO and Atlantic tripole. Climate dynamics, 46(7-8), 2269-2285.

Kucharski, F., Kang, I. S., Farneti, R., & Feudale, L. (2011). Tropical Pacific response to 20th century Atlantic warming. Geophysical Research Letters, 38(3).

Kucharski, F., Ikram, F., Molteni, F., Farneti, R., Kang, I. S., No, H. H., ... & Mogensen, K. (2016a). Atlantic forcing of Pacific decadal variability. *Climate Dynamics*, 46(7-8), 2337-2351.

Kucharski, F., Parvin, A., Rodriguez-Fonseca, B., Farneti, R., Martin-Rey, M., Polo, I., ... & Mechoso, C. R. (2016b). The teleconnection of the tropical Atlantic to Indo-Pacific sea surface temperatures on inter-annual to centennial time scales: a review of recent findings. Atmosphere, 7(2), 29.

Kushnir, Y. (1994). Interdecadal variations in North Atlantic sea surface temperature and associated atmospheric conditions. *Journal of Climate*, 7(1), 141-157.

Lee, S., & Kim, H. K. (2003). The dynamical relationship between subtropical and eddy-driven jets. Journal of the Atmospheric Sciences, 60(12), 1490-1503.

Li, C., & Wettstein, J. J. (2012). Thermally driven and eddy-driven jet variability in reanalysis. Journal of Climate, 25(5), 1587-1596.

Li, X., Xie, S. P., Gille, S. T., & Yoo, C. (2016). Atlantic-induced pan-tropical climate change over the past three decades. Nature Climate Change, 6(3), 275.

Lyu, K., & Yu, J. Y. (2017). Climate impacts of the Atlantic Multidecadal Oscillation simulated in the CMIP5 models: A re-evaluation based on a revised index. Geophysical Research Letters, 44(8), 3867-3876.

Madec, G., & Imbard, M. (1996). A global ocean mesh to overcome the North Pole singularity. Climate Dynamics, 12(6), 381-388.

Madec, G. the NEMO team (2016), Nemo ocean engine, version 3.6 stable. Note du P^ole de mod elisation de l'Institut Pierre-Simon Laplace, (27).

Madonna, E., Li, C., Grams, C. M., & Woollings, T. (2017). The link between eddy-driven jet variability and weather regimes in the North Atlantic-European sector. Quarterly Journal of the Royal Meteorological Society, 143(708), 2960-2972.

Madrigal-González, J., Ballesteros-Cánovas, J. A., Herrero, A., Ruiz-Benito, P., Stoffel, M., Lucas-Borja, M. E., ... & Zavala, M. A. (2017). Forest productivity in southwestern Europe is controlled by coupled North Atlantic and Atlantic Multidecadal Oscillations. Nature communications, 8(1), 2222.

Mantua, N. J., & Hare, S. R. (2002). The Pacific decadal oscillation. Journal of oceanography, 58(1), 35-44.

Mariotti, A., & Dell'Aquila, A. (2012). Decadal climate variability in the Mediterranean region: roles of large-scale forcings and regional processes. Climate Dynamics, 38(5-6), 1129-1145.

Marullo, S., Artale, V., & Santoleri, R. (2011). The SST multidecadal variability in the Atlantic–Mediterranean region and its relation to AMO. Journal of Climate, 24(16), 4385-4401.

McCabe, G. J., Palecki, M. A., & Betancourt, J. L. (2004). Pacific and Atlantic Ocean influences on multidecadal drought frequency in the United States. Proceedings of the National Academy of Sciences, 101(12), 4136-4141.

McGregor, S., Timmermann, A., Stuecker, M. F., England, M. H., Merrifield, M., Jin, F. F., & Chikamoto, Y. (2014). Recent Walker circulation strengthening and Pacific cooling amplified by Atlantic warming. Nature Climate Change, 4(10), 888.

Meehl, G. A., Arblaster, J. M., Fasullo, J. T., Hu, A., & Trenberth, K. E. (2011). Model-based evidence of deep-ocean heat uptake during surface-temperature hiatus periods. Nature Climate Change, 1(7), 360.

Meehl, G. A., & Teng, H. (2014). Regional precipitation simulations for the mid-1970s shift and early-2000s hiatus. Geophysical Research Letters, 41(21), 7658-7665.

Menary, M. B., Hodson, D. L., Robson, J. I., Sutton, R. T., Wood, R. A., & Hunt, J. A. (2015). Exploring the impact of CMIP5 model biases on the simulation of North Atlantic decadal variability. Geophysical Research Letters, 42(14), 5926-5934.

Miles, T., Glenn, S. M., & Schofield, O. (2013). Temporal and spatial variability in fall storm induced sediment resuspension on the Mid-Atlantic Bight. Continental Shelf Research, 63, S36-S49.

Miles, M. W., Divine, D. V., Furevik, T., Jansen, E., Moros, M., & Ogilvie, A. E. (2014). A signal of persistent Atlantic multidecadal variability in Arctic sea ice. *Geophysical Research Letters*, 41(2), 463-469.

Monahan, A. H., & Fyfe, J. C. (2006). On the nature of zonal jet EOFs. Journal of climate, 19(24), 6409-6424.

Nakamura, H., & Sampe, T. (2002). Trapping of synoptic-scale disturbances into the North-Pacific subtropical jet core in midwinter. Geophysical research letters, 29(16), 8-1.

Neale, R. B., Chen, C. C., Gettelman, A., Lauritzen, P. H., Park, S., Williamson, D. L., ... & Marsh, D. (2012). Description of the NCAR atmospheric model: CAM5. Tech. Rep. NCAR/TN-486+ STR.

O'Reilly, C. H., Woollings, T., & Zanna, L. (2017). The dynamical influence of the Atlantic Multidecadal Oscillation on continental climate. Journal of Climate, 30(18), 7213-7230.

Oleson, K., Lawrence, D., Bonan, G., Drewniak, B., Huang, M., Koven, C., ... & Swenson, S. (2013). Technical description of version 4.5 of the Community Land Model (CLM), 420 pp., doi: 10.5065.

Otterå, O. H., Bentsen, M., Drange, H., & Suo, L. (2010). External forcing as a metronome for Atlantic multidecadal variability. Nature Geoscience, 3(10), 688.

Peings, Y., & Magnusdottir, G. (2014). Forcing of the wintertime atmospheric circulation by the multidecadal fluctuations of the North Atlantic Ocean. Environmental Research Letters, 9(3), 034018.

Peings, Y., & Magnusdottir, G. (2016). Wintertime atmospheric response to Atlantic multidecadal variability: Effect of stratospheric representation and ocean–atmosphere coupling. Climate dynamics, 47(3-4), 1029-1047.

Ramankutty, N. (1994). An oscillation in the global climate system of period 65-70 years. *Nature*, 367(6465), 723-726.

Ruprich-Robert, Y., Msadek, R., Castruccio, F., Yeager, S., Delworth, T., & Danabasoglu, G. (2017). Assessing the climate impacts of the observed Atlantic multidecadal variability using the GFDL CM2. 1 and NCAR CESM1 global coupled models. Journal of Climate, 30(8), 2785-2810.Schlesinger, M. E., &

Ruprich-Robert, Y., Delworth, T., Msadek, R., Castruccio, F., Yeager, S., & Danabasoglu, G. (2018). Impacts of the Atlantic Multidecadal Variability on North American Summer Climate and Heat Waves. Journal of Climate, 31(9), 3679-3700.

Schlesinger, M. E., & Ramankutty, N. (1994). An oscillation in the global climate system of period 65–70 years. Nature, 367(6465), 723.Steinman, B. A., Mann, M. E., & Miller, S. K. (2015). Atlantic and Pacific multidecadal oscillations and Northern Hemisphere temperatures. Science, 347(6225), 988-991.

Steiger, N. J., Smerdon, J. E., Cook, E. R., & Cook, B. I. (2018). A reconstruction of global hydroclimate and dynamical variables over the Common Era. Scientific data, 5, 180086.

Sun, C., Li, J., & Zhao, S. (2015). Remote influence of Atlantic multidecadal variability on Siberian warm season precipitation. Scientific reports, 5, 16853.

Sun, C., Kucharski, F., Li, J., Jin, F. F., Kang, I. S., & Ding, R. (2017). Western tropical Pacific multidecadal variability forced by the Atlantic multidecadal oscillation. Nature communications, 8, 15998.

Sutton, R. T., & Hodson, D. L. (2005). Atlantic Ocean forcing of North American and European summer climate. *Science*, 309(5731), 115-118.

Sutton, R. T., & Hodson, D. L. (2007). Climate response to basin-scale warming and cooling of the North Atlantic Ocean. Journal of Climate, 20(5), 891-907.

Sutton, R. T., & Dong, B. (2012). Atlantic Ocean influence on a shift in European climate in the 1990s. *Nature Geoscience*, 5(11), 788-792.

Terray, L., & Cassou, C. (2002). Tropical Atlantic sea surface temperature forcing of quasi-decadal climate variability over the North Atlantic–European region. Journal of Climate, 15(22), 3170-3187.

Thompson, D. W., & Wallace, J. M. (2001). Regional climate impacts of the Northern Hemisphere annular mode. Science, 293(5527), 85-89.

Thompson, D. W., Lee, S., & Baldwin, M. P. (2003). Atmospheric processes governing the northern hemisphere annular mode/North Atlantic oscillation. Geophysical Monograph-American Geophysical Union, 134, 81-112.

Ting, M., Kushnir, Y., Seager, R., & Li, C. (2009). Forced and internal twentieth-century SST trends in the North Atlantic. *Journal of Climate, 22*(6), 1469-1481.

Ting, M., Kushnir, Y., Seager, R., & Li, C. (2011). Robust features of Atlantic multi-decadal variability and its climate impacts. *Geophysical Research Letters*, 38(17).

Trenberth, K. E., Branstator, G. W., Karoly, D., Kumar, A., Lau, N. C., & Ropelewski, C. (1998). Progress during TOGA in understanding and modeling global teleconnections associated with tropical sea surface temperatures. Journal of Geophysical Research: Oceans, 103(C7), 14291-14324.

Trenberth, K. E., & Shea, D. J. (2006). Atlantic hurricanes and natural variability in 2005. *Geophysical Research Letters*, 33(12).

Tyrlis, E., & Hoskins, B. J. (2008). The morphology of Northern Hemisphere blocking. Journal of the Atmospheric Sciences, 65(5), 1653-1665.

Uppala, S. M., Kållberg, P. W., Simmons, A. J., Andrae, U., Bechtold, V. D. C., Fiorino, M., ... & Li, X. (2005). The ERA-40 re-analysis. Quarterly Journal of the royal meteorological society, 131(612), 2961-3012.

Voldoire, A., Sanchez-Gomez, E., y Mélia, D. S., Decharme, B., Cassou, C., Sénési, S., ... & Déqué, M. (2013). The CNRM-CM5. 1 global climate model: description and basic evaluation. Climate Dynamics, 40(9-10), 2091-2121.

Wang, C., Dong, S., Evan, A. T., Foltz, G. R., & Lee, S. K. (2012). Multidecadal covariability of North Atlantic sea surface temperature, African dust, Sahel rainfall, and Atlantic hurricanes. *Journal of Climate*, 25(15), 5404-5415.

Wang, C., Zhang, L., Lee, S. K., Wu, L., & Mechoso, C. R. (2014). A global perspective on CMIP5 climate model biases. *Nature Climate Change*, 4(3), 201-205.

Wang, J., Kessler, J., Bai, X., Clites, A., Lofgren, B., Assuncao, A., ... & Leshkevich, G. (2018). Decadal variability of Great Lakes ice cover in response to AMO and PDO, 1963-2017. Journal of Climate, (2018).

Wittenberg, A. T., Rosati, A., Lau, N. C., & Ploshay, J. J. (2006). GFDL's CM2 global coupled climate models. Part III: Tropical Pacific climate and ENSO. Journal of Climate, 19(5), 698-722.

Wittman, M. A., Charlton, A. J., & Polvani, L. M. (2005). On the meridional structure of annular modes. Journal of climate, 18(12), 2119-2122.

Woollings, T., Hannachi, A., & Hoskins, B. (2010a). Variability of the North Atlantic eddy-driven jet stream. Quarterly Journal of the Royal Meteorological Society, 136(649), 856-868.

Woollings, T. (2010b). Dynamical influences on European climate: an uncertain future. Philosophical Transactions of the Royal Society of London A: Mathematical, Physical and Engineering Sciences, 368(1924), 3733-3756.

Woollings, T., Czuchnicki, C., & Franzke, C. (2014). Twentieth century North Atlantic jet variability. Quarterly Journal of the Royal Meteorological Society, 140(680), 783-791.

Woollings, T., Barnes, E., Hoskins, B., Kwon, Y. O., Lee, R. W., Li, C., ... & Spensberger, C. (2018). Daily to decadal modulation of jet variability. Journal of Climate, 31(4), 1297-1314.

Yeager, S. G., & Robson, J. I. (2017). Recent progress in understanding and predicting Atlantic decadal climate variability. Current Climate Change Reports, 3(2), 112-127.

Yuan, T., Oraiopoulos, L., Zelinka, M., Yu, H., Norris, J. R., Chin, M., ... & Meyer, K. (2016). Positive Low Cloud and Dust Feedbacks Amplify Tropical North Atlantic Multidecadal Variability.

Zanchettin, D., Bothe, O., Graf, H. F., Omrani, N. E., Rubino, A., & Jungclaus, J. H. (2016). A decadally delayed response of the tropical Pacific to Atlantic multidecadal variability. Geophysical Research Letters, 43(2), 784-792.

Zhang, R., & Delworth, T. L. (2006). Impact of Atlantic multidecadal oscillations on India/Sahel rainfall and Atlantic hurricanes. Geophysical Research Letters, 33(17).

Zhang, R., & Delworth, T. L. (2009). A new method for attributing climate variations over the Atlantic Hurricane Basin's main development region. *Geophysical Research Letters*, 36(6).

Zhang, L., & Wang, C. (2013). Multidecadal North Atlantic sea surface temperature and Atlantic meridional overturning circulation variability in CMIP5 historical simulations. *Journal of Geophysical Research: Oceans*, 118(10), 5772-5791.

Zhang, L., & Delworth, T. L. (2015). Analysis of the characteristics and mechanisms of the Pacific Decadal Oscillation in a suite of coupled models from the Geophysical Fluid Dynamics Laboratory. Journal of climate, 28(19), 7678-7701.

Zhang, R., Sutton, R., Danabasoglu, G., Delworth, T. L., Kim, W. M., Robson, J., & Yeager, S. G. (2016). Comment on "The Atlantic Multidecadal Oscillation without a role for ocean circulation". Science, 352(6293), 1527-1527.